Reviewed Preprint
v1 • December 5, 2025
Not revised

Reviewed Preprint
v2 • May 6, 2026
Revised by authors

Junctional and Actomyosin Dynamics Drive Endothelial Cell Rearrangements during Vascular Tube Formation

Ludovico Maggi[1], Jianmin Yin[1,*], Cora Wiesner[1,†], Ilkka Paatero[1,‡], Julian Malchow[2,§], Christian Helker[2], Markus Affolter[1], Heinz-Georg Belting[1]

[1]Biozentrum, Universität Basel, Basel, Switzerland • [2]Abteilung Entwicklungsbiologie, Phillipps-Universität, Marburg, Germany

For correspondence:
yinjm@scut.edu.cn
markus.affolter@unibas.ch
heinz-georg.belting@unibas.ch

*, †, ‡, § **Author notes:** See page 22

Funding: See page 22

Reviewing editor: Benjamin M Hogan, Peter MacCallum Cancer Centre, Australia

eLife Assessment

This **valuable** study focuses on a unique morphogenetic module, the junction-based lamellipodia (JBL). It provides a biomechanical understanding of how JBLs control endothelial cell-cell junctional remodelling to generate lumenised, multicellular blood vessels. The manuscript represents a robust, thoughtfully executed, and **convincing** study that uses high-resolution time-lapse imaging combined with pharmacological treatments to advance our understanding of lumen formation in vascular development.

https://doi.org/10.7554/eLife.109264.2.sa4

Abstract

Lumen formation is a key process during the morphogenesis of tubular organs such as the vertebrate vascular network. At the cellular level, lumen formation can be achieved by cell shape changes or cell rearrangements. We have previously shown that such cell rearrangements are driven by oscillating membrane protrusions, called junction-based lamellipodia (JBL), which provide a ratchet mechanism driving convergent cell movements to connect local lumens and generate vascular patency. By performing *in vivo* time-lapse imaging at high spatiotemporal resolution, we have analyzed the cytoskeletal and junctional dynamics, which underlie JBL formation and function. We show that JBL formation requires the activity of the F-actin nucleation complex Arp2/3. We further show that a novel junction is formed at the distal end of the JBL from a pool of VE-cadherin originating from outside the initial JBL area.

Subsequently, proximal and distal junctions merge and fuse, a process driven by actomyosin contractility. Prior to this fusion we observe a specific recruitment Myl9 within the interjunctional space. Furthermore, inhibition of actomyosin contractility abrogates junctional merging. Taken together, our analyses demonstrate that JBL constitute a module, which by alternate generation of pushing forces (JBL formation) and pulling forces (junctional merging) provide the physical means of endothelial cells to elongate and to rearrange and thereby generate a continuous vascular lumen.

Introduction

Vascular networks are formed by an array of morphogenetic processes, such as sprout outgrowth, anastomosis and pruning, which depend on the tight coordination of dynamic endothelial cell behaviors (Betz et al., 2016; Ellertsdóttir et al., 2010; Phng, 2018; Schuermann et al., 2014). In order to transport blood, the newly formed blood vessels need to form a continuous lumen. Studies of lumen formation in mammalian and zebrafish embryos have revealed that the early blood vessels of the trunk are formed by different morphogenetic processes. The larger axial vessels, the dorsal aorta (DA) and posterior cardinal vein (PCV), form their lumens between coalescing endothelial cells, a process referred to as cord hollowing (Ellertsdóttir et al., 2010; Jin

et al., 2005; Strilić et al., 2009; Zeeb et al., 2010). *In vivo* time-lapse analyses of the formation of the intersomitic vessels (ISV) and the dorsal longitudinal anastomotic vessels (DLAV) in zebrafish have revealed the existence of two alternative mechanisms of lumenization. In one mechanism, called transcellular lumen formation, the luminal cell membrane invaginates into the cell. This cell hollowing process is driven by blood pressure and results in so-called seamless tubes, which contain a lumen surrounded by single cells (Betz et al., 2016; Gebala et al., 2016; Herwig et al., 2011 ; Lenard et al., 2013; Phng and Belting, 2021). Alternatively, local lumens, which are formed between individual cells within a sprout can be fused by cell rearrangements (Herwig et al., 2011; Sauteur et al., 2014). Such endothelial cell rearrangements generate multicellular tubes (Betz et al., 2016; Phng and Belting, 2021). Studies examining lumenization of ISV and DLAV have shown that transcellular lumen formation requires blood pressure and that, in the absence of blood flow, endothelial cell rearrangements appear to be the default mechanism of vascular tube formation (Herwig et al., 2011; Lenard et al., 2013).

Endothelial cells are very motile - they can move within the angiogenic sprout and also in patent vessels in the presence of blood flow (Blum et al., 2008; Franco et al., 2016; Jakobsson et al., 2010). A dynamic balance between endothelial cell-cell adhesion and plasticity allows angiogenic sprouting while maintaining the endothelial seal. Previous analysis on blood vessel formation and anastomosis in zebrafish has shown that junctional remodeling is central to many aspects of morphogenetic endothelial cell-cell interactions. In particular, the adhesion molecule VE-cadherin (Cdh5) is essential for coordinated cell shape changes during multicellular tube formation, as loss of VE-cadherin was shown to inhibit cell rearrangements (Sauteur et al., 2014). Furthermore, rather than supporting a passive role of VE-cadherin, which is consistent with the maintenance of vascular integrity, an active force-generating function for VE-cadherin in this process was suggested (Sauteur et al., 2014). By performing *in vivo* high-resolution time-lapse imaging and genetic analyses, we have shown that endothelial cells use oriented, oscillating junction-based lamellipodia (JBL) to move over each other, which thus provide the physical means for cell rearrangements to drive multicellular tube formation (Paatero et al., 2018).

To better understand the cellular and molecular mechanisms of JBL function we have undertaken a detailed analysis of junctional and actomyosin dynamics. Taken together, our data show that JBL provide forward movement by generating pushing and pulling forces at the poles of junctional rings thereby elongating the cell and promoting cell rearrangements.

Results

Junction-based lamellipodia generate luminal connectivity

Lumenization of vascular sprouts is central to blood vessel formation. Although different morphogenetic mechanisms of vascular tube formation have been described, *in vivo* analysis in zebrafish embryos has established cord hollowing as the default mechanism of blood vessel formation in the absence of blood flow (Herwig et al., 2011; Lenard et al., 2013). During the cord hollowing process neighboring cells form local lumens which become interconnected via cell rearrangements (Andrew and Ewald, 2010). To visualize the relationship between JBL dynamics and endothelial cell rearrangements, we used two different transgenic reporters: EGFP-ZO1 to label EC junctions and UCHD-mRuby to label F-actin in junctions as well as in JBL protrusions (Figure 1a, b). Time-lapse analysis revealed that JBL formed in front of elongating junctions as the junctional rings move towards each other. As a consequence of these movements, the junctional rings merge and the converging cells form a new contact leading to the fusion of the previously separated luminal pockets (Figure 1c, d) (Herwig et al., 2011). In order to visualize the fusion of such luminal pockets we followed the localization GFP-Podxl, which labels the apical cell membrane, together with F-actin reporter UCHD-mRuby2, to delineate endothelial cell-cell junctions and F-actin base protrusions (Figure 1c). Time-lapse recordings revealed that fusion of apical membrane compartments occured within a few hours upon initiation of DLAV formation and was associated with junctional rearrangements between the three associated cells (Figure 1c, d and video s2). In agreement with our previous work, higher temporal resolution imaging

showed that cell junctions formed transient F-actin-based protrusion (JBL) at the pole with respect to junctional ring elongation (Figure 1 c, d and video s1, and video s3) (Paatero et al., 2018).

JBL form distal junctions by *de novo* recruitment of VE-cadherin

We have previously shown that JBL are oscillating protrusions, which drive junction elongation and thereby cell rearrangements during tube formation. A salient feature of JBL is the formation of a distal junction in front of the JBL (Paatero et al., 2018).

To gain more insight into the dynamics of distal junction formation, we compared the distribution of F-actin (Ruby-UCHD) with that of VE-cadherin (VE-cad-Venus) and ZO1 (EGFP-ZO1), respectively (Figure 2). Time-lapse experiments revealed distinct and dynamic localization of these proteins. During early phases of JBL formation VE-cadherin was diffusely distributed throughout the protrusion and accumulated in aggregates leading to a characteristic “double junction” pattern at the distal tip of the junctional ring (Figure 2a and video s4). Compared to VE-cadherin and ZO1 the early demarcation of F-actin at proximal and distal junction was less sharp (Figure 2 b, c and videos s5, s6). However, early aggregates of VE-cadherin and ZO1 were always positive for Ruby-UCHD, showing that these three proteins were present from the onset of distal junction formation. At subsequent stages, as the distal becomes more mature, ZO1 and VE-cadherin at the proximal junction were maintained, while the Ruby-UCHD signal started to fade (Figure 2 c-e).

Formation of the distal junction may occur in different ways. On one hand, it may form by a local junctional disassembly, followed by a reaggregation at the distal end of the JBL. This would essentially consist of a junctional rearrangement process. On the other hand, the distal junction may form *de novo* by recruitment of VE-cadherin from pools outside of the proximal junction. In order to distinguish between these scenarios, we performed color conversion experiments (Supplementary Figure 1 and video s7). Pools of photoconvertible VE-cadherin (Cdh5-mClav2) were differentially labeled by exposure to UV light within a narrow region of interest at the pole of the junctional ring (Supplementary Figure 1a), which resulted in efficient green-to-red conversion of fluorescence (Supplementary Figure 1 b). When we followed subsequent JBL dynamics over time, we noted that converted (red) VE-cad was absent from the protrusion as well as from the distal junction (Supplementary Figure 1c and video s7. representative of different 5 experiments). Instead, the distal junction contained nonconverted VE-cadherin. This indicates that the Ve-cad pool residing in the proximal junction does not substantially contribute to the JBL nor the distal junction but rather that the distal junction is formed *de novo* by recruitment of VE-cadherin from pools outside the proximal junction.

Arp2/3 complex dynamics spatiotemporally correlates with JBL formation

Membrane protrusions emerging from endothelial junctions are commonly seen in developing and newly formed blood vessels in the zebrafish embryo. Cell culture experiments, using human umbilical cord endothelial cells (HUVEC), have shown that such lamellipodial structures can control monolayer integrity and vascular permeability (Alves et al., 2018; Martinelli et al., 2013). In particular, so-called junction-associated intermittent lamellipodia (JAIL) are prominent in sub-confluent HUVEC, where they serve to repair junctional gaps (Taha et al., 2014). In contrast to JAIL, JBL are highly polarized relative to the vessel axis and they drive cell rearrangements rather than maintaining vascular integrity (Paatero et al., 2018). However, both lamellipodial structures are similar in their emergence from and association with endothelial cell junctions.

JAIL formation appears to be triggered by a local reduction in junctional tension and requires the activation of the ARP2/3 complex. To examine the role of the Arp2/3 complex in JBL formation, we used a reporter expressing Arpc1b-Venus fusion protein in the zebrafish vasculature. Arpc1b is an integral subunit of the active Arp2/3 complex and has previously been used as a reporter to

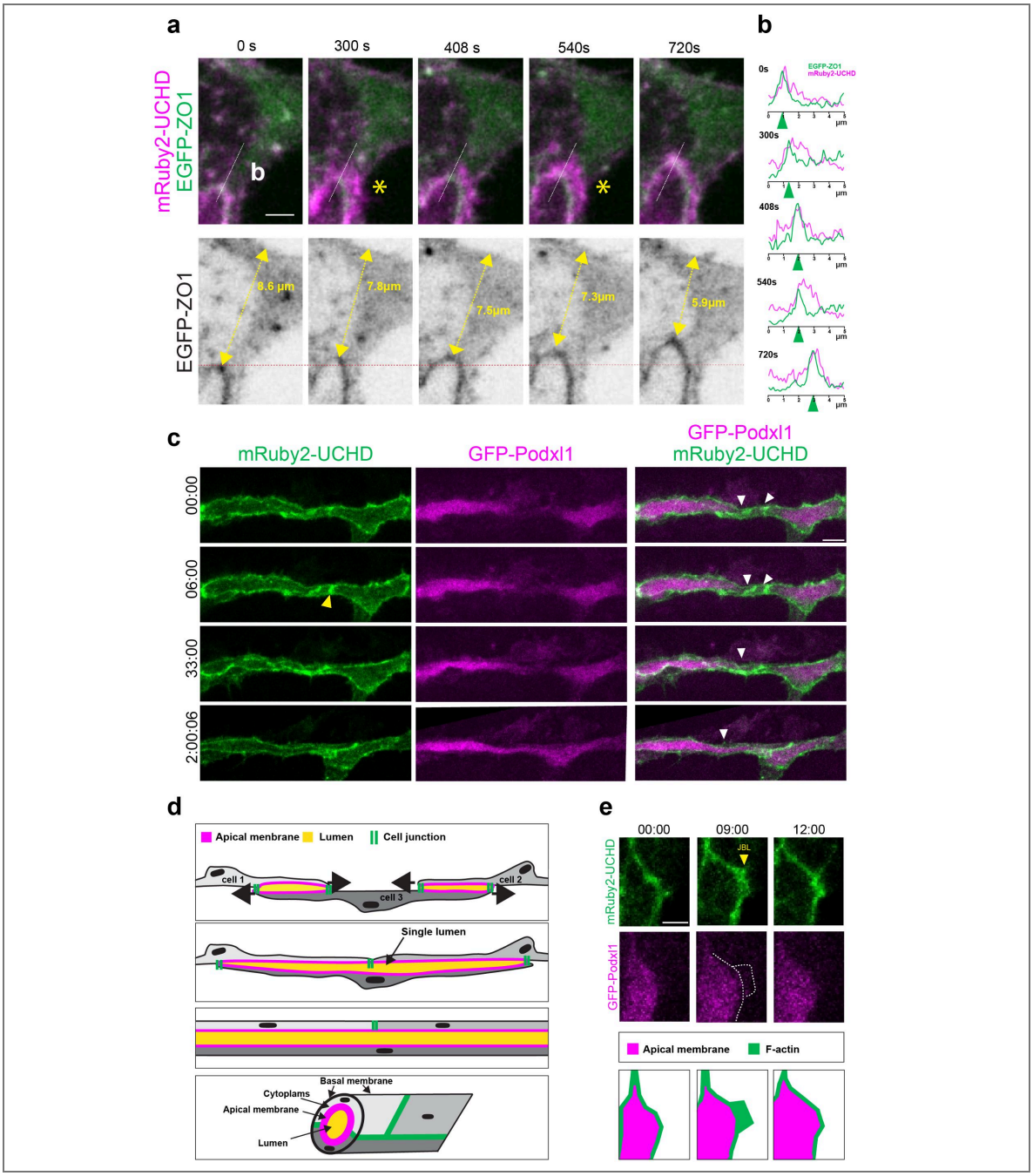

Figure 1. JBL generate luminal connectivity.

a: High-resolution time-lapse video (video s1) of EGFP-ZO1 and mRuby2-UCHD during junctional rearrangements. Yellow asterisks point to JBL. Yellow doubleheaded arrows indicate the distance between the junction and the dorsal end of the DLAV. **b:** Plots displaying the signal intensities of EGFP-ZO1 and mRuby2-UCHD, along the white lines, at different time points, during several JBL cycle. **c:** still images of time-lapse video (video s2) showing EGFP-Podxl1 and mRuby2-UCHD during luminal fusion, starting at approximately 32 minutes. The leading edges of the converging junctions are indicated by white arrowhead. Yellow arrowheads point to JBL. scale bar: 10 µm. **d:** Graphic depiction of blood vessel lumenization by cell convergence. Top: At first, cells 1 and 3 and cell 2 and 3, respectively, are forming cell-cell interfaces (cell junctions: green), which enclose local lumens (apical membrane: purple). Middle: JBL drive convergent cell movements, which lead to the formation of a novel cell contact (cells 1 and 2) and the merging of the two lumens into one (bottom). Graphic depiction of a lumenized DLAV, displaying the multicellular architecture. **e:** still images of time-lapse video s3 showing the oscillatory behavior of JBL (yellow arrowhead) during DLAV formation (30hpf). The white dashed line surrounds the UCHD-labeled JBL domain. scale bar: 5µm. A schematic representation of the time-lapse video is shown in the bottom panel.

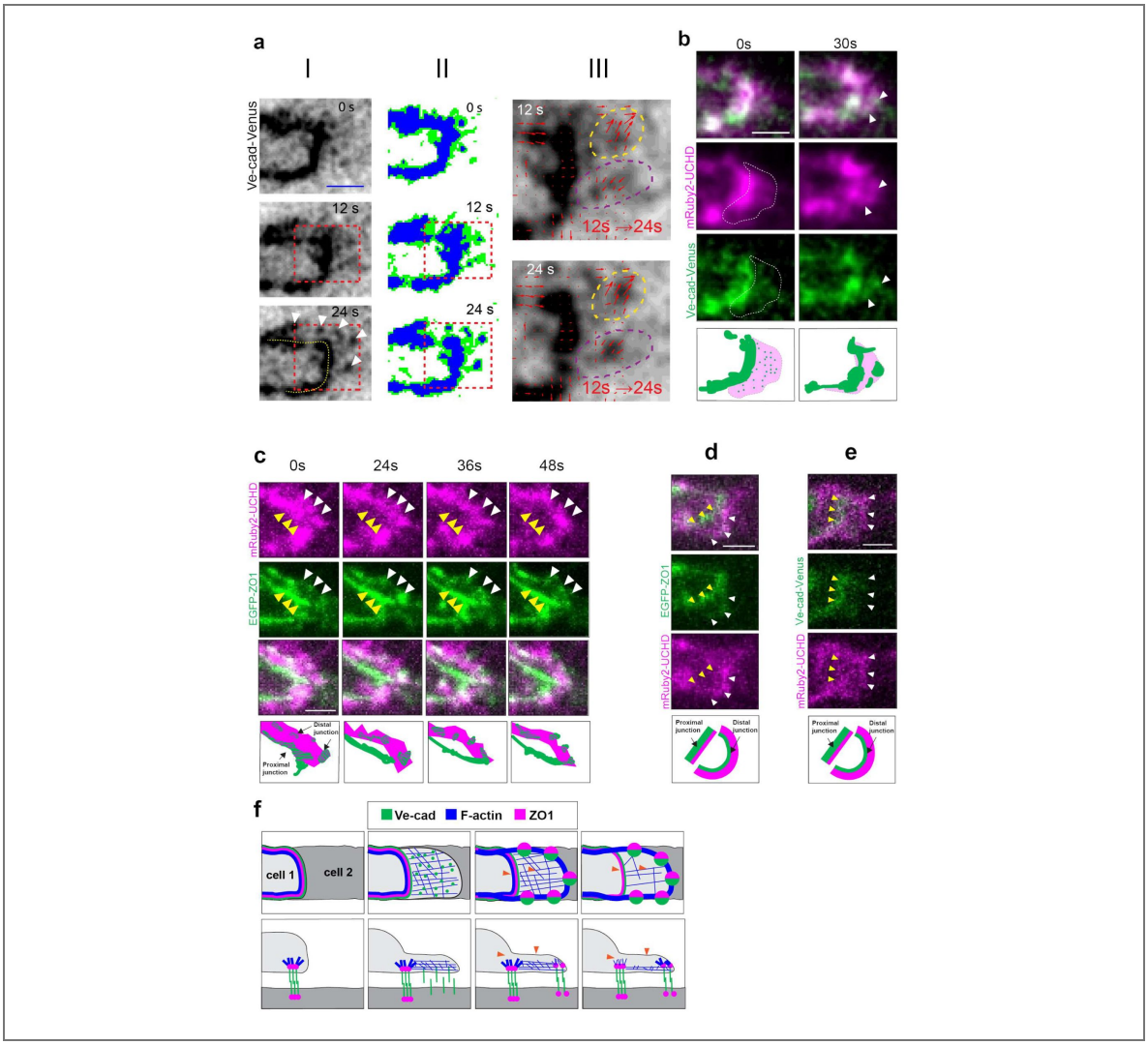

Figure 2. JBL form new junctions at the distal end of the membrane protrusion.

a: A (I)Time-lapse video (video s4) of VE-cad-Venus imaged at rate of 1stack/12s during distal junction formation. New distal junctions emerge in clusters at the distal end of the JBL. Ve-cad is diffusely localized in early JBL, while it accumulates in big foci at later time points. scale bar: 2 μm. (II) Three-level thresholding of a grayscale image. The original grayscale image (I) is segmented into three intensity levels: background (white), intermediate signal (green), and strong signal (blue). (III) Tracking of VE-cad aggregates from 12s to 24s. Particle trajectories are shown as arrows from 12 s to 24 s, with arrowheads indicating the direction of movement. Dashed circles highlight dynamic aggregation of VE-cad at distal junctions. White arrowheads point distal the junction. Yellow dashed line highlights the proximal junction. **b:** Still-images of time-lapse video showing mRuby2-UCHD and VE-cad-Venus during JBL (0s) and distal junction formation (30s). (video s5). The dashed line encircles the protrusion. White arrow heads point distal junction foci at the distal tip of the protrusion. scale bar: 2 μm. Similar observations were made in 15 videos. **c:** Still images of time-lapse video showing EGFP-ZO1 and mRuby2-UCHD during the presence of proximodistal junction. After distal junction formation, F-actin gradually diminishes from proximal junction and interjunctional space, while maintaining strong localization at the distal junction. Similar observations were made in 5 videos. White arrowheads confine UCHD expression domain. scale bar: 2 μM. Yellow and white arrowheads highlight proximal and distal junction respectively. **d,e:** Still image of EGFP-ZO1 and mRuby2- UCHD (D), and mRuby2-UCHD and VE-cad-Venus (E) respectively, in proximodistal junction. (video s6) While junctional proteins localize more strongly at the proximal junction, respect to the new, immature distal junction, F-actin faintly localizes at the proximal junction and strongly at the distal. Similar observations were made in 10+11 videos. Yellow and white arrowheads highlight proximal and distal junction respectively scale bar: 2 μm. **f:** Schematic representation the spatiotemporal distribution of VE-cad, F-actin and ZO1 during formation of the distal junction in top and side view: Initially VE-cad appears diffusely dispersed throughout the membrane protrusion. Distal junction foci form at the distal side of the lamellipodia. Actin network along the distal junction. Finally, the junctional actin network along the proximal junction dissappears, as depicted by orange arrow heads.

localize Arp2/3 activity in endothelial cells (Malchow et al., 2024; Padrick et al., 2011). Time-lapse analyses showed a discrete spatiotemporal deployment of Arp2/3 at the leading edge of the forming JBL (Figure 3). Imaging JBL over several oscillation cycles revealed that Arp2/3 accumulation coincided with the initiation and the elongation of JBL, while it disappeared at the end of each JBL cycle (Figure 3a and video s8). Comparison with ZO1 showed that Arp2/3 localized distally with no overlap within the proximal junction (Figure 3a). When we imaged Arp2/3 together with mRuby2-UCHD at higher temporal resolution (30s/frame), we observed that Arp2/3 was maintained at the leading edge of the membrane protrusion (Figure 3b, c and video s9). Taken together, these data show that Arp2/3 specifically marks the distal edge of the JBL during formation and elongation (Figure 3d).

As the above findings suggest that Arp2/3 is involved in JBL formation, we interfered with Arp2/3 function by pharmacological inhibition using CK666 (Hetrick et al., 2013). We used acute treatments to avoid secondary effects and performed live-imaging on rearranging endothelial cell junctions. Application of 0.2 mM CK666 at 32 hpf completely disrupted junctional Arp2/3 localization within 30 min. (Supplementary Figure 2). Analysis of F-actin organization revealed an increase of filopodia emanating from the junction in the area, which usually was occupied by JBL (Figure 4a-c and videos s10, s11). The abundance of these filopodia prevented the localization of JBL at the junctional poles - an observation consistent with previous cell culture studies (Henson et al., 2015), which suggests that filopodia are formed instead of lamellipodia in the absence of Arp2/3 activity. To verify that filopodia formation was caused by Arp2/3 inhibition, we performed wash-out experiments. Removal of the inhibitor from the medium effectively stopped filopodia formation at endothelial cell junctions, thus reverting the CK666 induced phenotype (supplementary Figure 3 and videos s12, s13). To test consequences of the loss of Arp2/3 activity on cell rearrangements, we measured the speed of junctional elongation in control and CK666 treated embryos. By imaging ZO1 labeled junctions over 1 hour we found that the speed of junction elongation was strongly reduced from an average of 8µm/h to 3µm/h (Figure 3 d,e and videos s14, s15). Taken together, the results show that JBL formation depends on Arp2/3 function and that the absence of Arp2/3 activity leads to a strong impairment of endothelial cell rearrangements during blood vessel formation.

Proximal and distal junctions resolve by junctional merging and fusion

The appearance of “double junctions” (consisting of a proximal and a distal junction) is a distinctive junctional feature observed in JBL. Their spatiotemporal dynamics suggest that they represent part of the mechanism by which JBL promote junction elongation. Live-imaging revealed a cyclic turnover between the two junctional states: single junction and double junction pattern. Time-lapse imaging of VE-cad-Venus at high temporal resolution showed that this turnover is mediated by the cyclic formation of the distal junction followed by the merging and fusion of the proximal and distal junctions (Figure 5a and video s16).

Myosin light-chain localization correlates with junctional merging

The cyclic junctional pattern in JBL suggests that it may represent a physical ratchet mechanism, which drives junction elongation. Therefore, we wanted to explore whether junctional mergence could be driven by actomyosin contractility. Increase in tension is accompanied by a recruitment of non-muscular myosin to the actomyosin cytoskeleton (Munjal et al., 2015). By coupling fluorescent reporters the myosin regulatory light chain dynamic changes of actomyosin tension can be visualized *in vivo* at subcellular resolution (Fernandez-Gonzalez et al., 2009). To monitor the spatiotemporal distribution of actomyosin contractility during JBL cycle, we utilized myosin regulatory light chain (MLC) (Myl9a-GFP and Myl9b-Cherry) as reporters for non-muscular myosin II (NMII) activity (Lancino et al., 2018). Myl9 accumulated along the junctions but was strongly enriched in JBL at both ends of the junctional ring (yellow arrowheads in Figure 5b).

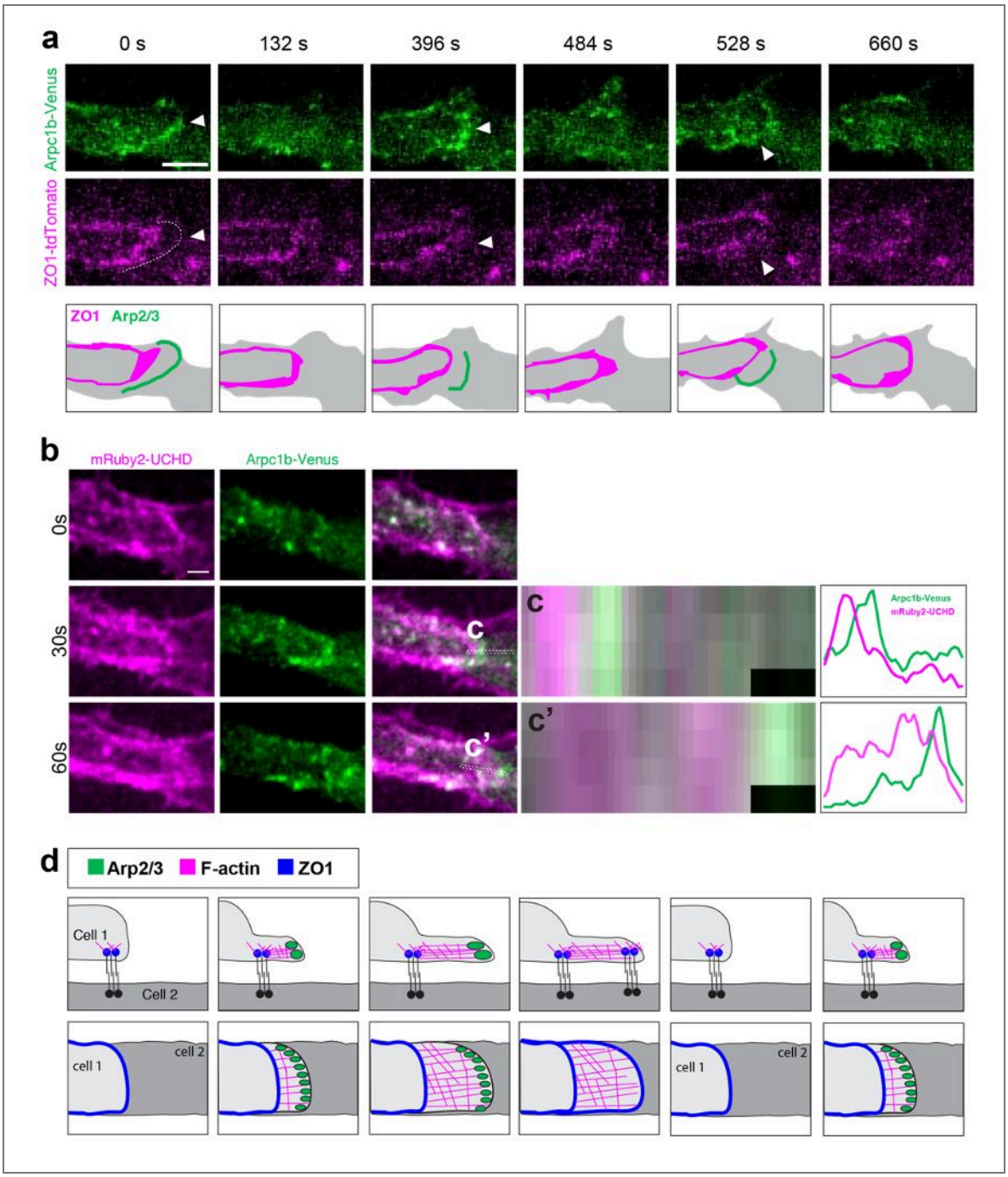

Figure 3. **Arp2/3 localization oscillates at the distal end of JBL.**

a: Time-lapse video (video s8) of Arpc1b-Venus and ZO1-tdTomato at about 30hpf, showing deposition of Arp2/3 at the distal side of the junctional ring during 2 JBL cycles. scale bars: 2 µm. **b:** Time-lapse video (video s9) of Arpc1b-Venus and mRuby2-UCHD during a JBL event. scale bar: 2 µm. **c** and **c':** Plots showing the average intensity of Arpc1b-Venus and mRuby2-UCHD along rectangular ROIs drawn along the JBL at 30 and 60 seconds, respectively. scale bar: 2 µm **d:** Schematic model of top and side view of spatiotemporal localization of ARP2/3, F-actin and ZO1 during JBL formation and extension for 1.5 JBL cycle.

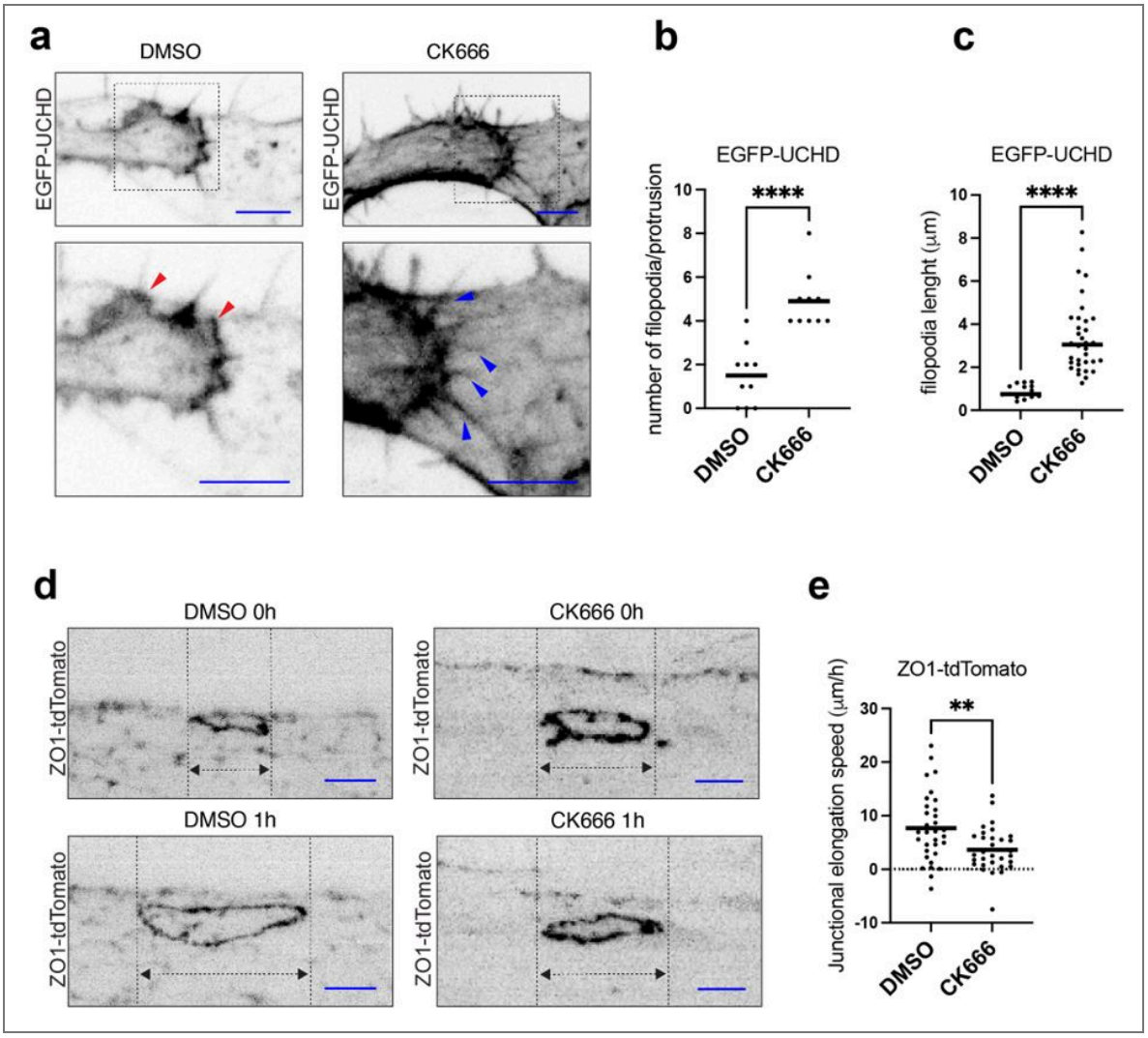

Figure 4. Arp2/3 activity is required for junctional elongation and JBL formation.

a: Still-images from time-lapse videos (videos s10, s11) of JBL labelled with EGFP-UCHD, at around 32hpf, in the presence of DMSO (1%) or 1h incubation with CK666 (200µM). Similar observations were made in 10 videos. scale bars: 5 µm. Similar observations were made in more than 12 videos. **b:** Quantification of number of filopodia/JBL in DMSO (1%), n=10 JBL and CK666 (200µM), n=10 JBL events. Unpaired t-test was used for statistical analysis. (p-value < 0.0001). **c:** Quantification JBL filopodia length in DMSO (1 %), n=15 JBL and CK666 (200 µM), n=34 JBL events. **d:** Still images from time-lapse videos (videos s14, s15) of a ZO1-tdTomato labeled junctional rings in the presence of DMSO (1%), CK666 (200µM). Top panels t =0 and bottom panels after 1h incubation. scale bars: 10µm. **e:** Quantification of the junctional elongation velocity in DMSO (1%), n=21 junctions (10) embryos) and CK666 (200 µM), n=24 (10 embryos). Dotted line indicated no movement observed, black lines are medians. Unpaired t-test was used for statistical analysis. (p-value = 0.0047).

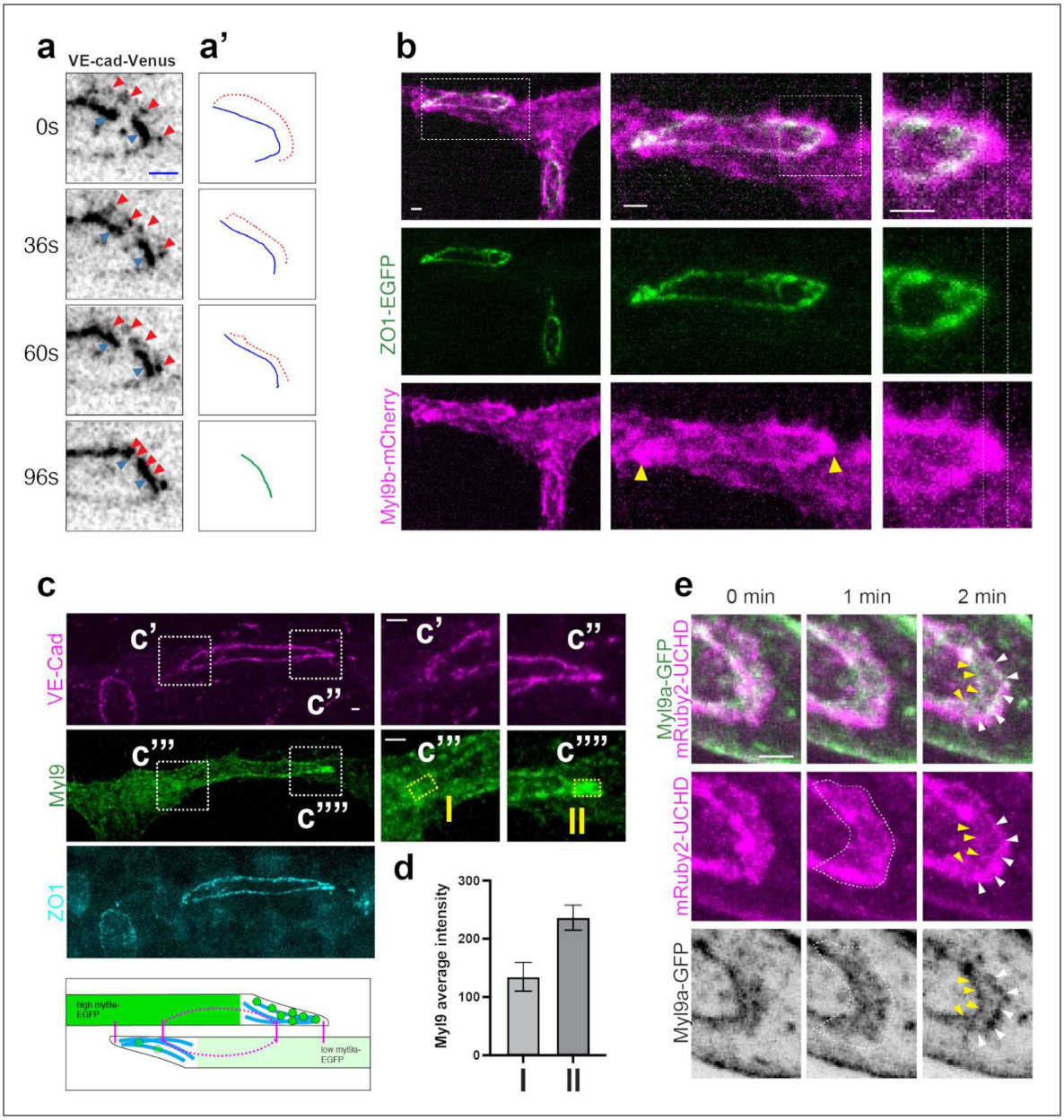

Figure 5. MLC is enriched at the junction poles.

a: Stills from time-lapse video (video s16) of VE-cad-Venus during junctional merging. Blue and red arrowheads point to the proximal and distal junction, respectively. The two junctions are gradually moving closer until they merge. Similar observations were made in 13 videos. scale bars 2 μm. **b:** Confocal image of ISV and DLAV of Myl9b-mCherry and ZO1-EGFP at around 32 hpf. Yellow arrowheads point to JBL. Dashed lines underline the distal expression domain of Myl9b-mCherry at the junctional pole. scale bars: 2 μm. **c:** Confocal image of DLAV and ISV immunofluorescence against GFP (green), VE-cad (magenta) and ZO1 (cyan) of an embryo expressing Myl9a-GFP at around 32hpf in a case of mosaic expression: the top cell has stronger Myl9a-GFP expression than the bottom cell (as in the schematic). **c', c'', c''', c''''** dashed squares delimitate JBL regions of the two cells. **d:** quantification of Myl9-EGFP average intensity the yellow dashed squares ROIs (I) and (II) drawn on the JBL domain. The error bars indicate standard deviation between pixel intensities within the square (area of interest). **e:** Still images of a time-lapse video s17 showing Myl9a-GFP and mRuby2-UCHD localization during JBL formation during anastomosis of the PCeV at around 60 hpf imaged with spinning disc. White dashed lines delineate the JBL region. Yellow and white arrowheads point to the proximal and distal junction, respectively. Myl9-GFP is enriched inside the lamellipodia and localizes at the distal junction at later time points. scale bars: 2 μm.

During cell rearrangements JBL are formed at each pole of the junctional ring in a complementary fashion: each JBL is formed by one of the interacting cells corresponding to the forward orientation with respect to cell movement (Paatero et al., 2018)(see schematic in Figure 5c). To test whether Myl9 accumulation corresponds to the forward orientation of the JBL, we analyzed rare mosaic situations in which Myl9a-GFP was expressed in only one of the partnering cells. Indeed, we observed high levels of Myl9a-GFP in JBL formed by the high-expressing cell pointing into the forward direction of the elongating junction (Figure 5c-d).

Vascular tube formation by cell rearrangements has also been described in other vascular beds. We turned to the posterior cerebral vein (PCeV), which is generated by JBL-driven cell rearrangements converting the initial tube architecture from unicellular to multicellular (Lenard et al., 2013). When we compared Myl9a-EGFP distribution to mRuby2-UCHD, we found that the former localized within the JBL adjacent to the forming distal junction of the JBL (see yellow arrowheads in Figure 5e and video s17).

In order to gain a better understanding how actomyosin contractility may drive junctional mergence, we imaged the distribution of Myl9 at high spatiotemporal resolution. We first used VE-cadherin-EGFP to label proximal and distal junctions as spatial landmarks and thus demarcate the area of interest for the quantification of Myl9b-mCherry in space and time (Figure 6a, b, Supplementary figure 4, and videos s18 - s22). We defined three areas - proximal junction, interjunctional and distal junction and quantified Myl9b-mCherry at two time-points (0” and 45”) at the onset and during junctional mergence, respectively (Figure 6b). These quantifications reveal a redistribution Myl9 from the proximal and distal junctions towards the interjunctional space (Figure 6c). This increase indicates a strong recruitment of Myl9 and a concomitant increase of actomyosin contractility within the area between the proximal and distal junctions.

Actomyosin contractility is required for junction elongation and junctional mergence

In order to assess the role of actomyosin contractility in junction elongation more directly, we used the Rock inhibitor Y-27632 (Uehata et al., 1997)and measured the length of junctional rings over 60 minutes. Rock inhibition strongly inhibited junction elongation compared to DMSO controls (Figure 7a, b and videos s23, s24). To test whether the lack of junction elongation under Rock inhibition may be caused by defects in JBL function, we performed acute short-term Y-27632 treatment and performed live-imaging over 30 minutes to image JBL dynamics during reduction of actomyosin contractility - with a focus on the merging of proximal and distal junctions. To this end, we imaged 20 (Y-27632) and 13 (DMSO) events of junctional merging, respectively, and tracked individual interjunctional distances over time (Figure 7c-e and videos s25, s26). Inhibition of actomyosin contractility led to a strong inhibition of junctional mergence, ranging from a reduction in speed to a complete block in junctional mergence. This blockage in junctional mergence was reflected by the overall increased occurrence of “double junctions” under Rock inhibition (20 (Y-27632) vs 13 events (DMSO-control) in 18 videos). Taken together, these results show that high levels of actomyosin contractility reside within interjunctional space and that these contractile forces are responsible for junctional mergence. Furthermore, these data suggest that JBL formation together with junctional mergence are the driving force of junctional elongation and endothelial cell rearrangements during angiogenic blood vessel formation.

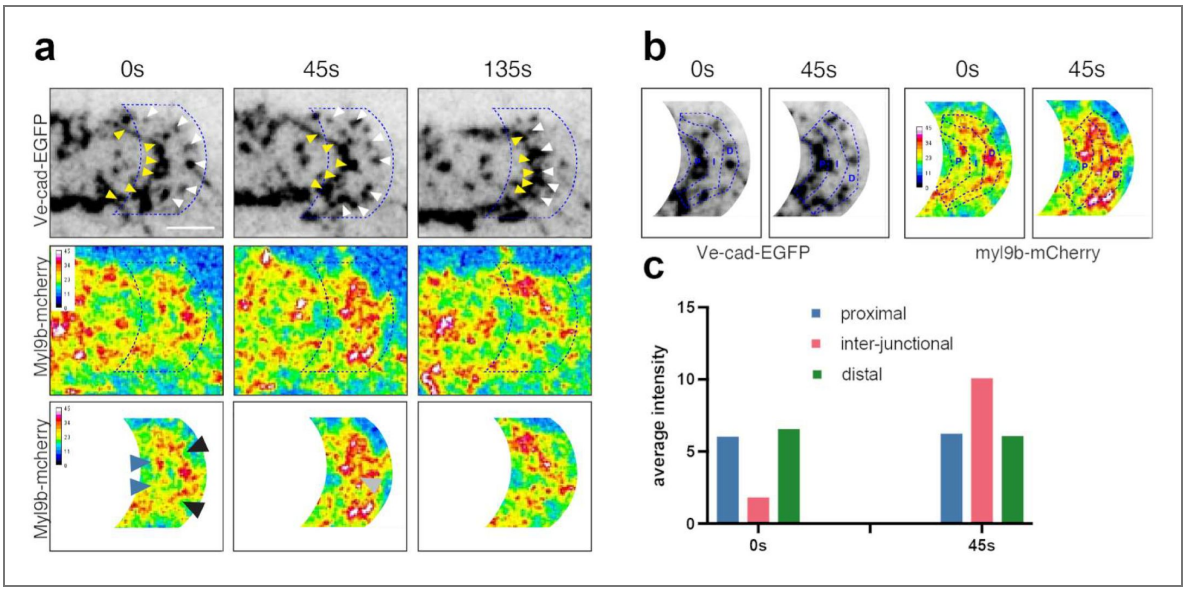

Figure 6. **Myosin light-chain dynamics correlates with junctional merging.**

a: Still pictures of time-lapse video (video s18) of VE-cad-EGFP (Cdh5ΔC-EGFP) and Myl9b-mCherry (shown in "fire"-LUT) during junctional merging. Blue dashed lines confine the applied mask. Yellow and white arrowheads point to the proximal and distal junction, respectively. Blue and black arrowheads point to MLC accumulation at proximal and distal junction. Similar observations were made in six videos. Gray arrowheads point to newly recruited inter-junctional Myl9-mCherry. Similar observations were made in nine videos. **b:** Dashed blue lines delimitate 3 regions: proximal junction region (P), distal junction region (D) and inter-junctional space (I). **c:** Plot of average intensity of Myl9b-mCherry in the three regions over time. Signal intensities have been corrected for background levels, which has been evaluated as average of average intensities in five rectangles in the cytoplasm. scale bars: 2 μm.

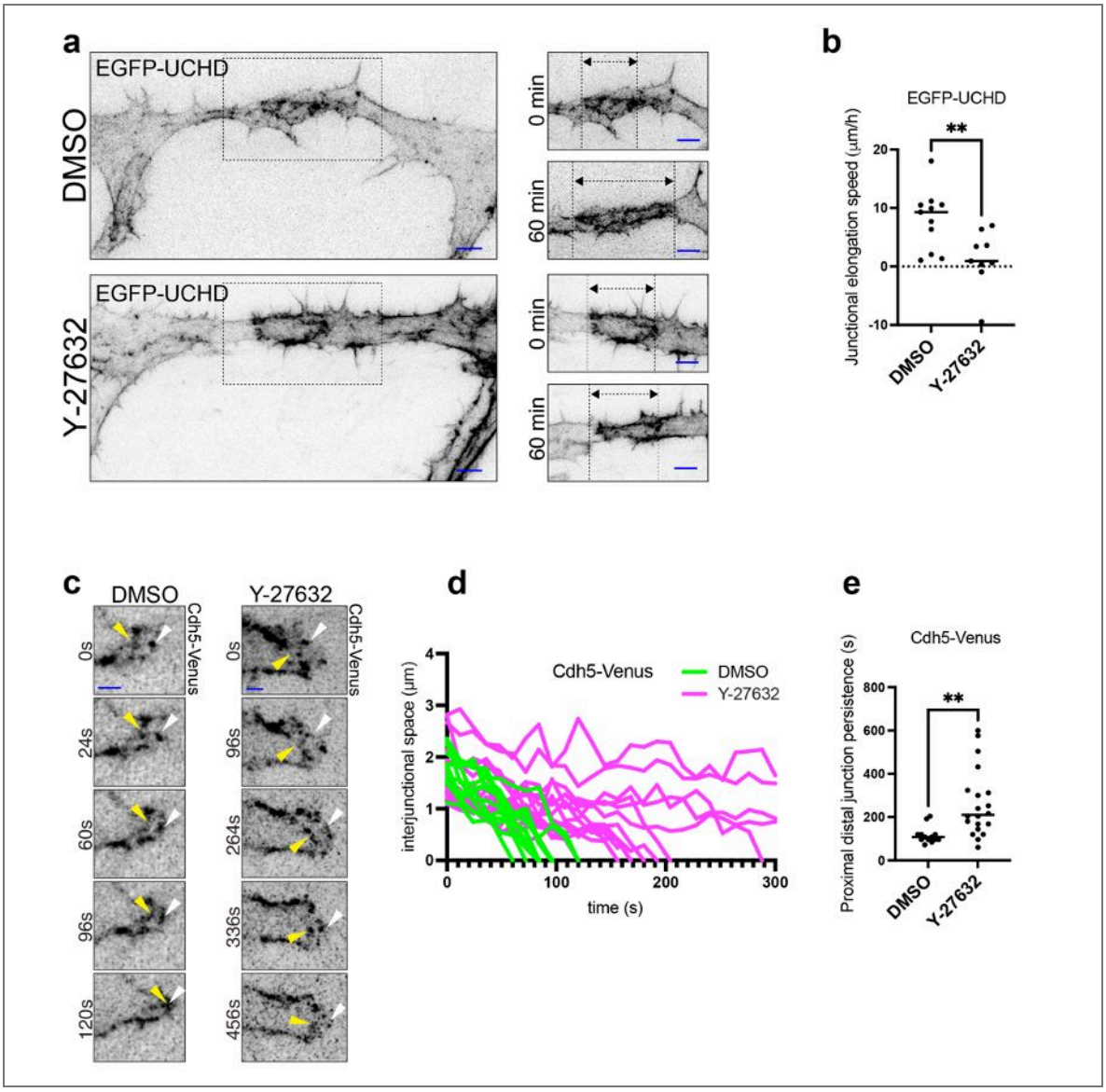

Figure 7. Actomyosin contractility drives junctional conversion.

a: Still images from time-lapse videos (videos s23 and s24) EGFP-UCHD labelled junctional rings around 32 hpf, in the presence of DMSO (1%) or Y-27632 (45 µM). Top panels t = 0 and bottom panels 60 min incubation. scale bar: 10µm. **b:** Quantification of the junctional elongation velocity in DMSO (1%), n =11 junctions and Y-27632 (45 µM), n = 8. Dotted line indicated no movement observed, black lines are medians. Unpaired t-test was used for statistical analysis. p-value = 0.0081. **c:** Stills images from timelapse videos (videos s25 and s26) VE-cad-Venus labelled proximodistal junction, during junctional merging in the presence of DMSO (1%) or Y-27632 (75 µM). White and yellow arrowheads are pointing distal and proximal junctions respectively. scale bar: 2µm. **d:** Tracking of proximal-distal junction distance over time of individual junctional merging events in DMSO (1%) (green lines), and Y-27632 (75 µM) treated embryos (magenta lines). **e:** Quantification of the persistence of proximal and distal junction in DMSO (1%), n=13 junctional merging events and Y27632 (75 µM) n=20. Unpaired t-test was used for statistical analysis. p-value = 0.0027.

Discussion

Lumen formation is key in the formation of tubular organs such as blood vessels. Endothelial cells can use different morphogenetic pathways to generate a lumen, including membrane invagination, cord hollowing or lumen ensheathment (Eberlein et al., 2021; Phng and Belting, 2021). The dorsal longitudinal anastomotic vessel (DLAV) of the zebrafish embryo can be formed by either membrane invagination or cell rearrangements, which result in unicellular and multicellular tubes, respectively (Betz et al., 2016; Phng and Belting, 2021). Here, we have analyzed the cell rearrangements, which connect small luminal pockets within the initial endothelial rod, thereby generating a continuous lumen in a fully patent vascular tube.

The coalescence of local, extracellular lumens is commonly observed during the cord hollowing process of different biological tubes, including the notochord of Ciona intestinalis, the vertebrate dorsal aorta as well as the neural tube and intestine (Bagnat et al., 2007; Dong et al., 2009; Gladysheva et al., 2021; Jin et al., 2005; Strilić et al., 2009). In those tubular organs, in which lumen coalescence has been analyzed, it was found that it is mainly caused by lumen expansion, which in turn is driven by directed liquid transport and hydrostatic pressure (Bagnat et al., 2007; Lowery and Sive, 2005; Munson et al., 2008; Navis and Bagnat, 2015). In contrast, the lumen coalescence observed in the zebrafish ISV, DLAV and PCeV is accomplished by active cell intercalation. That is, endothelial cells actively elongate their cell-cell junctions until they form novel cell-cell contacts, which allow the connection of the two adjacent lumens.

We have previously shown that endothelial junction elongation is driven by junction-based lamellipodia (JBL) (Paatero et al., 2018). Careful analysis of junctional and cytoskeletal reporters revealed that JBL dynamics can be subdivided into 4 discrete steps: 1) JBL formation, 2) formation of a new, distal junction, 3) junction conversion and 4) junction stabilization (Paatero et al., 2018). Taken together, these studies showed that JBL provide an oscillating ratchet-like mechanism, in which endothelial cells employ F-actin-based protrusions and VE-cadherin-mediated cell-cell contacts to move over each other. JBL thus provide the physical means for cell rearrangements to drive multicellular tube formation.

In this study we have further explored the junctional and actomyosin dynamics to discern how JBL generate the motive force required for junction elongation and cell rearrangements. In essence, our data show that JBL require ARP2/3 dependent Factin polymerization for JBL formation as well as actomyosin contractility to merge the proximal and distal junctions at the end of the JBL cycle. Thus, by sequential deployment of pushing (F-actin polymerization) and pulling (junction merging) forces, JBL promote forward movement of endothelial cells (summarized in Figure 8).

Oscillatory junctional protrusions of endothelial cells have also been described in cultured HUVECs (Cao et al., 2017; Taha et al., 2014). Here, so-called junction-associated intermittent lamellipodia (JAIL) form in similar intervals as JBL. However, differences in junctional dynamics suggest that JAIL and JBL represent related but distinct cellular activities. JAIL formation is thought to be triggerered by local dissolution of endothelial adherens junctions (i.e. by downregulation of VE-cadherin). Subsequently, these protrusions retract EC junctions are re-established (Cao et al., 2017; Taha et al., 2014). In this experimental paradigm, JAIL do not promote endothelial cell movement. JBL, in contrast, provide endothelial motility during blood vessel morphogenesis. Furthermore, formation of JBL is not preceded by a dissolution of EC junctions and a distal junction is formed at the leading edge of the protrusion leading to a “double junction” configuration as an intermediate state. Our studies show that these “double junctions” are an integral part of the cellular mechanism of junction elongation. We have previously shown that JBL are most prominent during multicellular tube formation and become less prevalent and smaller thereafter (Paatero et al., 2018). These salient and distinct features prompted us to adopt the term junction-based-lamellipodia (JBL), in order to differentiate them from JAIL. Although JAIL have also been implicated in endothelial cell migration (Cao and Schnittler, 2019; Cao et al., 2017; Seebach et al., 2021) neither junctional patterns nor junctional dynamics

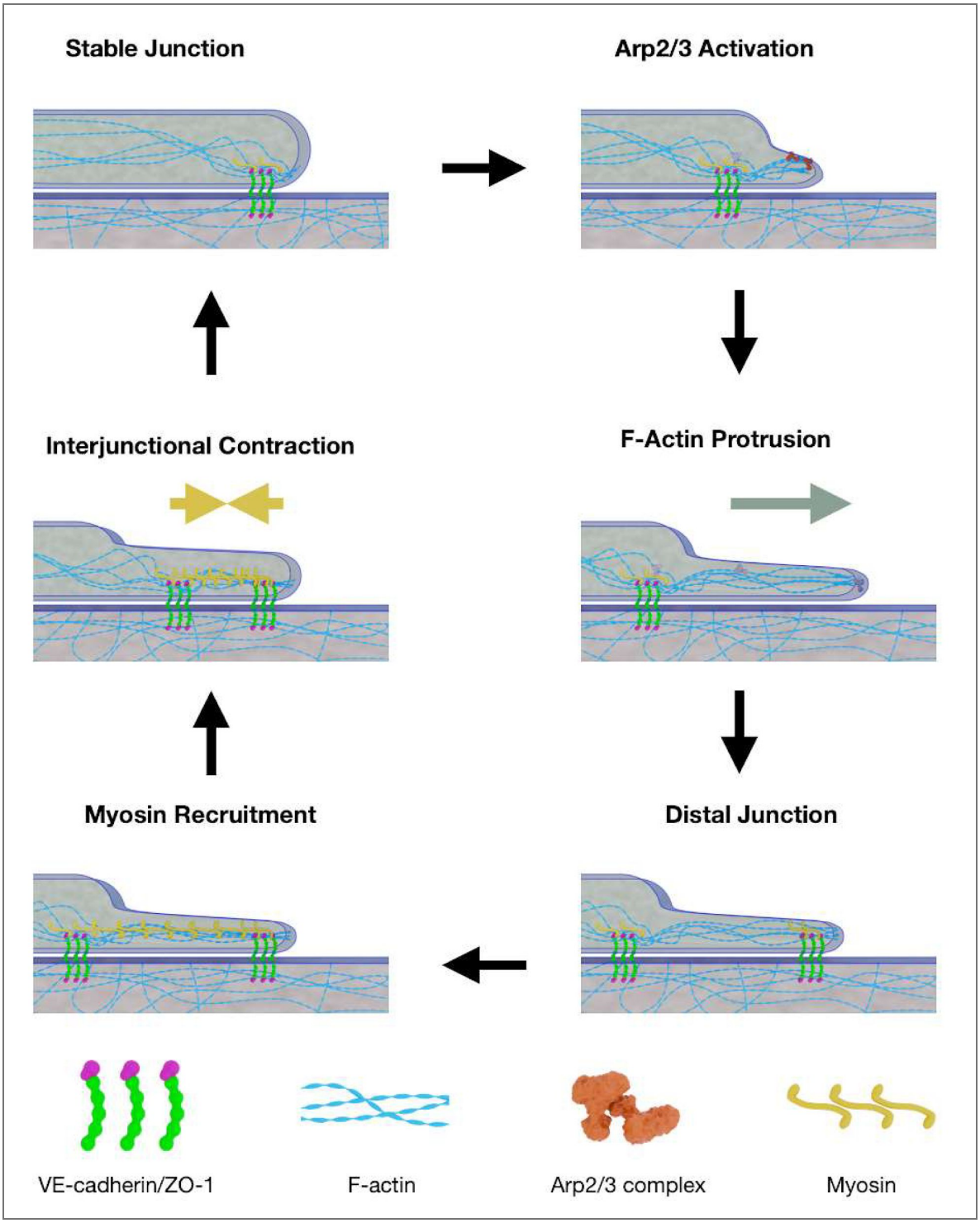

Figure 8. Schematic representation of the molecular mechanism of junction elongation by junction-based lamellipodia (JBL).

JBL formation is initiated by Arp2/3 activation. The JBL is pushed forward by F-actin polymerization. At the distal end a new cell-cell junction is formed. MyosinII is recruited to the interjunctional space. Actomyosin contraction merges the proximal and distal junctions resulting in an overall elongation of the junctional ring. See video s27.

have been analyzed in this context. Thus, JAIL and JBL represent similar but different lamellipodia-like protrusions. JAIL are associated with the maintenance of endothelial integrity, as well as the control permeability and trans-endothelial cell migration, as has been suggested by several publications (Cao et al., 2017; Kipcke et al., 2025; Seebach et al., 2021; Taha and Schnittler, 2014). In contrast, JBL drive cell rearrangements, by step-wise elongation of cell junctions resulting in convergent cell movements.

Lamellipodial structures resembling JBL, displaying double junctions, have recently been described in the oak leaf-shaped endothelial cells of dermal lymphatics in the mouse (Schoofs et al., 2025). Here, the double junctions are thought to regulate endothelial shape and in particular to stabilize the interendothelial cell overlap, which is important to control the interstitial fluid transport.

Our photoconversion experiments (see Supplementary Figure 1) show that the distal junction is formed *de novo* from VE-cadherin pools originating from outside the existing (proximal) junction. During distal junction formation, we observe that VE-cadherin forms clusters resembling spot-junctions observed in the context of organ morphogenesis in other systems. Consistent with our observation such spot-junctions have been shown to be important in the formation of contractile F-actin fibers in these systems (Lecuit et al., 2011). While we are currently not able to monitor actin flow in our experimental *in vivo* system, our observation that the formation of the distal junction coincides with the formation of a distal F-actin belt is consistent with a clutch mechanism, in which transligation of VE-cadherin triggers reorganization of the cortical actin cytoskeleton similar to what has recently been described in cell culture studies (Noordstra et al., 2023). Furthermore, our previous findings from zebrafish *cdh5* null mutants or embryos expressing a VE-cadherin protein (VE-cadΔCT) lacking the β-catenin binding site show that VE-cadherin mediated cell-cell interactions as well as VE-cad/F-actin interaction are important for JBL-driven junction elongation (Paatero et al., 2018; Sauteur et al., 2014).

The cell motility-promoting activity of VE-cadherin during tube formation may be quite unique, considering that in most studies cadherins have been described to stabilize epithelia, limit cell motility and to regulate contact inhibition of locomotion (Campàs et al., 2024; Maître and Heisenberg, 2013; Noordstra et al., 2023) Cadherin-based cell interactions have been shown to be essential for dynamic cell movements in several morphogenetic processes (Friedl and Mayor, 2017; Mayor and Etienne-Manneville, 2016). In the case of collective border cell migration during *Drosophila* oogenesis and migration of primordial germ cells in zebrafish, cadherins have been shown to provide traction for collective and single cell migration, respectively (Blaser et al., 2006; Cai et al., 2014).

A salient feature of JBL is their appearance at both ends of each rearranging cell. This bipolar activity causes the cells to elongate in both directions and rearrange rather than to migrate. Furthermore, and in contrast to lamellipodia-driven mechanisms of cell migration, the domain of actomyosin contractility is confined within the interjunctional area (between distal and proximal junctions, see Figures 6 and 8). This suggests that the restricted area of contractility is not only demarcated by the proximal and distal junctions, but that these junctions act as insulators to segregate compartments of different actomyosin tension along the cellular interface. We propose that this insulator function is essential to permit junction elongation.

In this study, we have investigated the cellular and molecular basis of force generation in JBL. Through detailed analysis of junctional, cytoskeletal, and regulatory proteins, we uncover a biphasic mechanism involving alternating protrusive and contractile forces. Notably, and in contrast to classical paradigms of cell migration, we show that actomyosin contractility is spatially restricted to a narrow zone at the junctional pole during endothelial cell movement. Together, our findings reveal a novel mechanism of cell rearrangement during vascular cord hollowing. JBL serve as localized modules that generate both protrusive and contractile forces during junctional remodeling and cell elongation. Moreover, JBL-localized junctions may act as insulators, spatially confining actomyosin tension to the junctional pole.

Material and Methods

REAGENT or RESOURCE	SOURCE	IDENTIFIER
Antibodies		
Mouse anti-human-ZO1	Thermo Fisher Scientific	Catalog # 33-9100 *RRID: AB 87181*
guinea pig anti-zebrafish-VE-cadherin	Paatero et al. (2018)	N/A
chicken anti-GFP	Abcam	RRID: ab13970
goat anti-guinea pig IgG-Alexa Flour 568	Thermo Fisher Scientific	Catalog # A-11075 RRID: *AB_2534119*
goat anti-mouse IgG-Alexa Flour 633	Thermo Fisher Scientific	Catalog # A-21050 RRID: *AB_2535718*
goat anti-chicken IgY-Alexa Fluor 488	Thermo Fisher Scientific	Catalog # A-11039 RRID: *AB_2534096*
Chemicals, peptides, and recombinant proteins		
Pierce Immunostain Enhancer	Thermo Fisher Scientific	CAT# 46644
Methylene Blue	Sigma-Aldrich	CAT#1.15943
Tricaine	Sigma-Aldrich	CAT# A5040
Proteinase K	Roche	CAT# 3115836001
Glyofixx	Thermo Fisher Scientific	CAT# 494437
Triton X-100	Sigma-Aldrich	CAT# 9036-19-5
Bovine Serum Albumin	Roche	CAT# 10735086001
Sodium azide	Sigma-Aldrich	CAT# S2002
1-phenyl-2-thiourea (PTU)	Sigma-Aldrich	CAT# P7629
Low melting point agarose	Sigma-Aldrich	CAT# A9414

Lead contact

Further information and request for resources and reagents should be directed and will be fulfilled by the Lead Contact; Heinz-Georg Belting (*heinz-georg.belting@unibas.ch*).

Materials availability

Materials and zebrafish lines generated and used in this study are available upon request to the lead contact.

Fish maintenance and stocks

Zebrafish (Danio rerio) were maintained according to FELASA guidelines (Aleström et al., 2020). All experiments were performed following institutional and ethical welfare guidelines and animal protocols in accordance with federal guidelines approved by the Kantonales Veterinäramt of Kanton Basel-Stadt (1027H, 1014HE2, 1014 G). Breeding and embryo collection were done according to standard protocols (Westerfield, 2007). Pain, distress, and discomfort were minimized as much as possible.

The following zebrafish lines were used in this study:

Name	RRIDs	Origin
Tg(fli:Gal4ff)^{ubs3}	RRID:*ZFIN_ZDB-ALT-120113-6*	(Herwig et al., 2011)

Tg(UAS:mRuby2-UCHD)^{ubs20}	RRID:*ZFIN_ZDB-ALT-190628-2*	(Paatero et al., 2018)
Tg(UAS:EGFP-UCHD)^{ubs18}	RRID:*ZFIN_ZDB-ALT-150316-3*	(Sauteur et al., 2014)
TgBAC(ve-cad:ve-cadTS)^{uq11bh}	RRID:*ZFIN_ZDB-ALT-181106-3*	(Lagendijk et al., 2017)
Tg(UAS:cdh5ΔC-EGFP)^{ubs60}	ZFINID:ZDB-TGCONSTRCT-130925-1	this study, (Lenard et al., 2013)
TgKI(tjp 1 a-tdTomato)^{pd1224}	ZFINID: ZDB-ALT-231027-18	(Levic et al., 2021)
Tg(fli1a:Arpc1b-m Venus-p2A-Arpc3-mTurq2)^{mr25}	ZFINID: ZDB-ALT-251006-8	(Malchow et al., 2024)
Tg(kdrl:Myl9a-GFP)^{ip5Tg}	ZFINID: ZDB-ALT-181115-10	(Lancino et al., 2018)
TgBAC(cdh5:cdh5-mClavGR2)^{ubs58}	ZFINID: ZDB-ALT-250403-1	(Yin et al., 2024)

Sex was not considered in this study because zebrafish embryos used for the experiments were at developmental stages prior to sex differentiation. Therefore, the sex of the embryos was not determined or relevant to the outcomes.

Live imaging of zebrafish embryos

In DLAV experiments, zebrafish embryos between 30 to 32 hpf were dechorionated and anaesthetized with 0.16mg/ml (1×) tricaine methanesulfonate (Sigma). The embryos were selected for presence of fluorescence and mounted into microwell dishes within 0.55% low-melting-point agarose (ROTI) and covered with E3 buffer containing 1× tricaine. In PceV experiments, transgenic embryos selected for presence of fluorescence were anaesthetized in 1 × tricaine (0.08%) and mounted in a 35 mm glass-bottom Petri dish (0.17 mm, MatTek), using 0.7% low melting agarose (Sigma) containing 0.08% tricaine and 0.003% 1-phenyl-2-thiourea (PTU; Sigma-Aldrich). The embryos were mounted into microwell dishes within 0.55% low-melting-point agarose (ROTI) and covered with E3 buffer containing 1 × tricaine.

A Leica SP5 confocal microscope with a 40x water immersion objective was used for live-imaging experiments. High spatiotemporal resolution time-lapse images were acquired with an Olympus SpinSR spinning disc microscope using a 60X silicon oil (NA = 1.3) objective, with a z-stack step size of 0.6 µm at different frequencies depending on the experiment.

Photoconversion experiments

Photoconversion experiments were performed using a Leica SP5 confocal microscope with a 40x water immersion objective (NA = 1.1). Photoconversions were applied to manually selected regions of interest (ROIs) with a 405 nm laser for 10–20 seconds to induce conversion, monitored by simultaneous imaging at 488 nm to ensure complete conversion. All the imaging was performed at 28.5 °C.

Junction elongation assay

Junctional elongation was assessed by measuring elongation speed of isolated junctional rings during DLAV formation between 30 and 32 hpf. Inhibitor treatments CK666 (200 µM), Y-27632 (75 µM), or DMSO (1%) were applied 1h before mounting of embryos into 0.55% low-melting point agarose. The same concentrations of chemicals were applied to the low-melting-point agarose mounting medium and the E3 medium on top of it before imaging and imaging the junctions for 60–90 min on a Leica SP5 (Y-27632) Olympus SpinSR spinning disc microscope or Olympus SpinSR spinning disc (CK666) microscope.

Junctional merging tracking

Speed of junctional merge was evaluated by monitoring isolated junctional rings during DLAV formation. Inhibitor treatment Y-27632 (75 µM) or DMSO (1%) were applied 30 min before mounting. The same concentrations of chemicals were applied to the low-melting-point agarose mounting medium and the E3 medium on top of it before imaging and imaging the junctions for

10–15 min on Olympus SpinSR spinning disc microscope. Distances were measured using Fiji software. In each frame, the interjunctional distance was defined as the maximum distance between the proximal and distal junctions. A line was manually drawn between the proximal and distal junctions in Fiji, and its length was recorded. The same proximal and distal junction landmarks were used consistently across all time points.

Immunostaining

Zebrafish embryos of 30 to 32 hpf were fixed after dechorionation using Glyofixx (Thermo-Fisher Scientific) and incubated at 4°C overnight (ON) in 1.5 ml Eppendorf tubes (max. 20 embryos per tube). After fixation, embryos were washed four times for 5 minutes in 1x PBST at room temperature (RT) on a rocking platform. Embryos were then permeabilized using 0.5–1 % Triton-X100 in PBST for 30 min at RT. They were then blocked with 2% BSA and 5% goat serum in PBST overnight with continuous shaking at 4 °C. After blocking, the primary antibody solution was added. The primary antibodies were either diluted in blocking solution or Pierce Immunostain Enhancer Solution (Thermo Fisher Scientific). Primary antibody incubation was performed at 4 °C for 3 days. After incubation, the solution was removed, and the embryos were washed at least four times for 30 minutes each with PBST at 4 °C, or overnight. Subsequently, the embryos were incubated with secondary antibodies, diluted 1:2000 in blocking solution, and incubated at 4 °C.

Image preparation and analysis

Image analysis and measurements were performed using FIJI RRID:*SCR_002285*. Z-stacks were flattened by *maximum slice intensity projections*. Where needed, noise was reduced using Gaussian filtering (radius 0.7) and/or background subtracted (rolling ball radius 50) using ImageJ RRID:*SCR_003070*. Contrast and brightness of images were linearly adjusted. Particle Image Velocimetry (PIV) was employed to measure velocity fields in fluid flow as previously described (Yin et al., 2024). Image panels were created using the Open Microscopy Environment (OMERO). ARP2/3- Venus and mRuby2-UCHD localization were evaluated on a 4pixel-wide rectangle, and the average over length, corrected for background (evaluated as average of average intensity in 5 rectangles on the cell cytoplasm) and displayed in a graph using Graphpad Prism 10.4.1 RRID:*SCR_002798*. Proximal, distal, and interjunctional space domains were defined using VE-cad distribution, My9-mcherry distribution was evaluated as average intensity in the distinct domains The intensities are corrected for background (which has been evaluated as average of average intensities in 5 rectangles in the cell cytoplasm) and displayed in a graph using Graphpad Prism 10.4.1.

Statistical analysis

GraphPad Prism 10.4.1 was used to perform statistical analyses. For every experiment and analysis, sample size is specified in the figure legend. Sample sizes were not pre-determined using statistical methods, and all data meeting the quality control criteria were included in the analyses. Randomization was not applied to the experiments. Unless specified otherwise, default settings were used for all software tools in the analyses. Whenever a p-value is presented in the text or figures, the corresponding statistical test is indicated.

Supplementary Figures

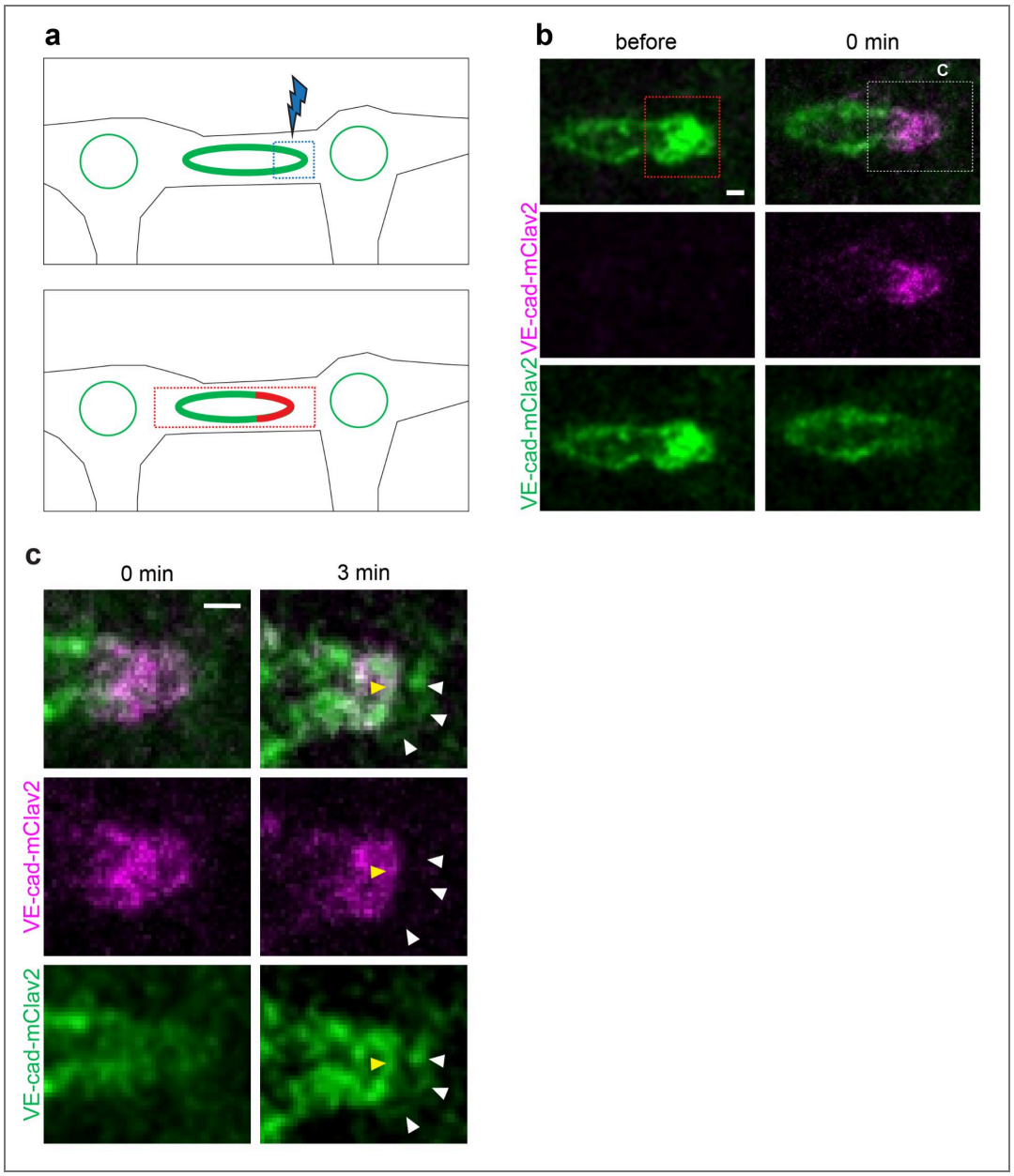

Supplementary Figure 1. **The distal junction forms *de novo*. a:** Schematic representation of the experimental design. VE-cad-mClav2 is photoconverted at one pole of the junctional ring. Then time lapse imaging is performed on the half-converted ring. **b:** Time-lapse images (video s7) showing a DLAV junctional ring of an embryo expressing VE-cad-mClav2 before and right-after photoconversion. The red dashed square delimitates the photoconverted area. The white dashed square demarcates the zoomed-in area of c. **c:** Time-lapse of the zoomed in junctional ring pole. right-after photoconversion and 4 min later. White and yellow arrowheads point distal and proximal junction respectively. Distal junction is labeled by green, non-photoconverted VE-cad; but not by red photoconverted VE-cad. scale bars: 5µm.

Supplementary Figure 2. CK666 disrupts Arp2/3 localization in DLAV anastomotic junctions.

Stills of Arpc1b-Venus and ZO1-td tomato before (**a, c**) and after 30 min treatment with DMSO 1 % (**c**) (n=17) and CK666 200 µM (**d**) (n=25). Timepoint 0 is around 30 hpf n>20. White arrow heads are pointing at junctional poles. **a', b', c', d'** are magnifications of the white dashed square delimited areas. scale bar: 10µm.

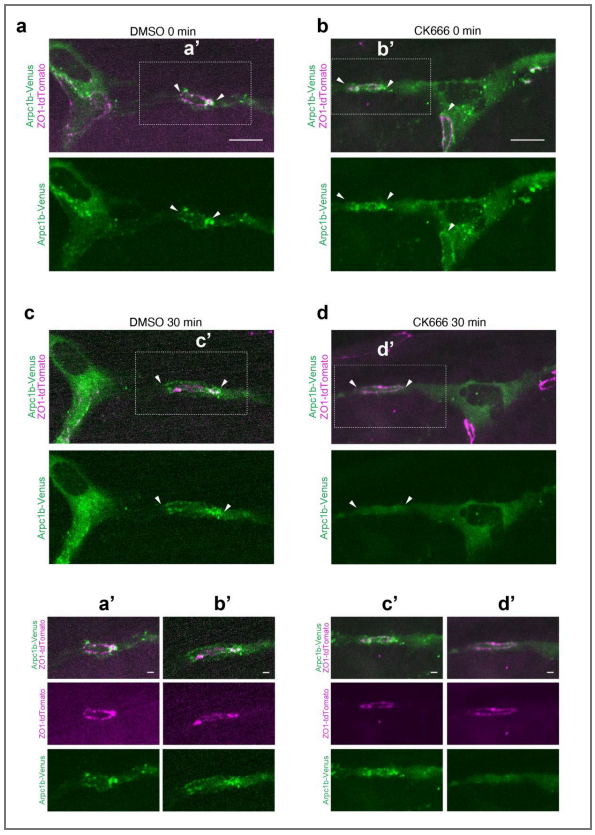

Supplementary Figure 3. CK666 mediated JBL inhibition is reversible upon washout.

a: Still images from time-lapse videos (videos s12 and s13) showing F-actin dynamics at the same junctional ring, labeled with EGFP-UCHD, at around 30hpf (left) and 32hpf (right), after 30 min incubation with CK666 (200µM), and after a 90 min washout, respectively. scalebar 2µm. Similar observation were made in 11 movies. Blue and red arrowheads point to ectopic filopodia under CK666 inhibition and and reemerging lamellipodia during washout, respectively. **b:** Quantification of number of filopodia/JBL in CK666 (200 µM), n=11 JBL and washout n=17 JBL events. Unpaired t-test was used for statistical analysis. (P value = 0.0003). **C**: Quantification JBL filopodia length in CK666 (200 µM), n=11 JBL and washout n=17 JBL events. Unpaired t-test was used for statistical analysis. (p-value < 0.0001).

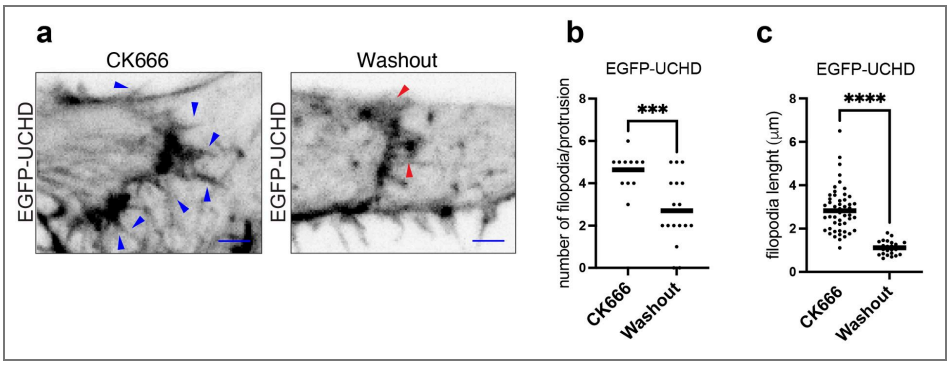

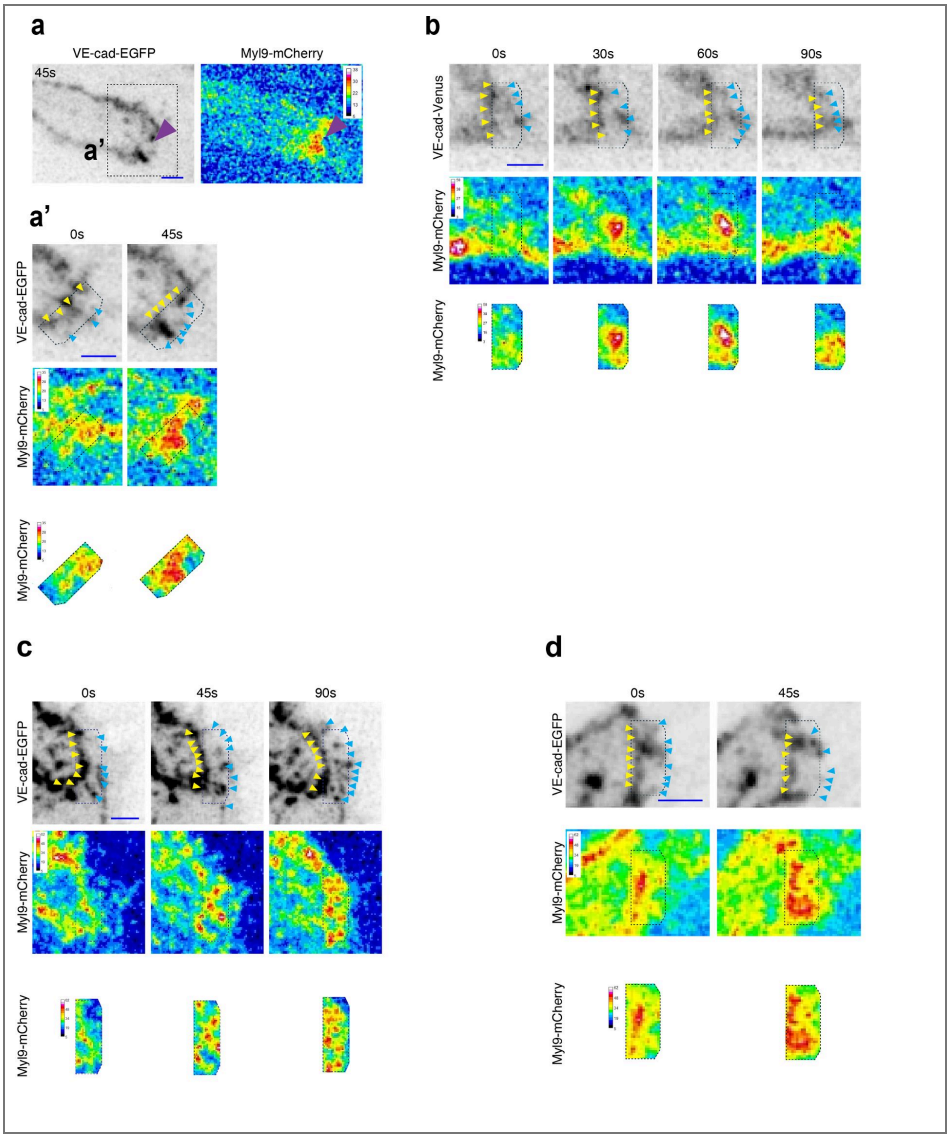

Supplementary Figure 4. Myosin light-chain recruitment at the inter-junctional space during merging.

a, a': Time-lapse of VEcad-EGFP (Cdh5ΔC-EGFP) and Myl9b-mCherry (shown in "fire" LUT) during "double junction" state (video s17). **a:** Still-image showing polarized accumulation of MLC during ''double junction'' state. **a'**: Still-images showing recruitment of MLC between proximal and distal junction. Yellow and blue arrowheads highlight the proximal and distal junction respectively **b:** Still-images from time-lapse video s18 of VE-cad-Venus and Myl9b-mCherry showing increase of MLC in the inter-junctional space prior to proximodistal junction mergence. Yellow and blue arrowheads highlight the proximal and distal junction. **c, d:** Time-lapses of VE-cad-EGFP (Cdh5ΔC-EGFP) and Myl9b-mCherry videos s19 and s20 showing recruitment of MLC between proximal and distal junction during ''double junction'' state. Yellow and blue arrowheads highlight the proximal and distal junction, respectively. scale bars: 2μm.

Data availability

The data that support the findings of this study are available in the supporting information of this article. *https://www.researchsquare.com/article/rs-7065344/v2*

Acknowledgements

We thank Kumuthini Kulendra and Andre Rodriguez for fish care and the Imaging Core Facility of the Biozentrum (Universität Basel) for microscopy support. We thank Anne Schmid (Institute Pasteur, Paris, France) for providing *Tg(kdrl: Myl9a-GFP)*^{p5Tg} and Michel Bagnat (Duke University, USA) for providing *TgKI(tjp1a-tdTomato)*^{pd1224}. We thank Sven Andreas Belting for preparing illustrations and graphic animations. This work has been supported by the Kantons Basel-Stadt and Basel-Land and by grants from the Swiss National Science Foundation (310030_200701 and 310030B_176400) to M.A..

Additional information

Author contributions

M.A. and H.-G.B. conceptualized the project. L.M., J.Y., C.W., I.P. and H.-G.B. designed the experiments. L.M., J.Y., C.W. and I.P. performed experiments and analyzed the data. J.M. and C.H. generated *Tg(flia:Arpc1b-mVenus-p2A-Arpc3- mTurq2)*^{mr25}. L.M. and H.-G.B. wrote the manuscript. M.A., L.M. and H.-G.B edited the manuscript. All authors reviewed the manuscript.

Funding

Funder	Grant reference number	Author
Schweizerischer Nationalfonds zur Förderung der Wissenschaftlichen Forschung (SNF)	310030_200701	Markus Affolter
Schweizerischer Nationalfonds zur Förderung der Wissenschaftlichen Forschung (SNF)	310030B_176400	Markus Affolter

Author ORCID iDs

Ludovico Maggi: https://orcid.org/0000-0002-9543-7840
Jianmin Yin: https://orcid.org/0000-0002-2966-8739
Ilkka Paatero: https://orcid.org/0000-0001-5926-2396
Christian Helker: https://orcid.org/0000-0003-0427-5338
Markus Affolter: https://orcid.org/0000-0002-5171-0016
Heinz-Georg Belting: https://orcid.org/0000-0002-1538-4364

Author notes

Jianmin Yin: Current address: Medical School at South China University of Technology (SCUT), Guangzhou, China
Cora Wiesner: Current address: Botnar Foundation, Campus ETHZ Basel, Basel, Switzerland
Ilkka Paatero: Current address: Turku Bioscience Centre, University of Turku and Åbo Akademi University, Turku, Finland
Julian Malchow: Current address: Institut für Physiologische Chemie, Universität Münster, Germany
Competing interests: The authors declare no competing interests.

Additional files

Figure 1 - video s1. JBL drive endothelial cell movements. Time-lapse video of EGFP-ZO1 and mRuby2-UCHD at around 30hpf. Actin-rich protrusions (mRuby2-UCHD) form at the front of the elongating junction (EGFP-ZO1). Yellow asterisks point to JBL. Yellow double-headed arrows indicate the distance between the junction and the dorsal end of the DLAV. Scale bar: 10µm

Figure 1 - video s2. JBL drive local lumen fusion. Time-lapse video showing EGFP-Podxl1 (labeling apical cell membrane) and mRuby2-UCHD (labelling F-actin) during DLAV formation, starting at approximately 32 hpf. The leading edges of the converging junctions are indicated by white arrowhead. Yellow arrowheads point to JBL. Scale bar: 10 µm.

Figure 1 - video s3. JBL form adjacent to the apical cell compartment. Time-lapse video showing the oscillatory behavior of JBL (F-actin protrusions labeled with mRuby2-UCHD (green), yellow arrowhead) during DLAV formation (30hpf). The apical compartment is labeled by EGFP-Podxl1 (magenta). The white dashed line surrounds the UCHD-labeled JBL domain. Scale bar: 5µm.

Figure 2 - video s4. Formation of a new junction at the distal end of the JBL. Time-lapse of VE-cad-Venus imaged at rate of 1stack/12s during distal junction formation. New distal junctions emerge in clusters at the distal end of the JBL. Ve-cad is diffusely localized in early JBL, while it accumulates in big foci at later time points. Scale bar: 2 µm.

Figure 2 - video s5. Formation of a new junction at the distal end of the JBL. Time-lapse video showing F-actin (mRuby2-UCHD, magenta) and VE-cad-Venus (green) during JBL protrusion (0s) and distal junction formation (30s). The dashed line encircles the protrusion. White arrow heads point distal junction foci at the distal tip of the protrusion. Scale bar: 2 µm.

Figure 2 - video s6. Formation of a new junction at the distal end of the JBL. Time-lapse video showing dynamic EGFP-ZO1 (green) and mRuby2-UCHD (magenta) distribution during distal junction formation in the forming DLAV (approx. 32 hpf). After distal junction formation, F-actin gradually diminishes from proximal junction and interjunctional space, while maintaining strong localization at the distal junction. Scale bar: 2 µM. Blue and white arrowheads highlight proximal (PJ) and distal junction (DJ), respectively.

suppl. Figure 1 - video s7. The distal junction forms *de novo*. Time-lapse video s7 showing a DLAV junctional ring of an embryo expressing VE-cad-mClav2 before (0 min) and right after photoconversion (1, 2, 3 min). The red square delimitates the photoconverted area. scale bar: 5µm.

Figure 3 - video s8. Arpc1b-Venus oscillations occur distal to the junction. Time-lapse video of Arpc1b-Venus (green) and ZO1-tdTomato (magenta) at about 30hpf, showing deposition of Arpc1b-Venus at the distal side of the junctional ring over two JBL cycles. Scale bar: 2 µm.

Figure 3 - video s9. Arpc1b localizes at the distal end of JBL. Time-lapse of Arpc1b-Venus (green) and mRuby2-UCHD (magenta) during the protrusion phase of a JBL. scale bar: 2 µm.

Figure 4 - video s10. Arp2/3 activity is required for JBL formation. Time-lapse video of JBL labelled with EGFP-UCHD, at around 32hpf, in the presence of DMSO (1%) (control). scale bar: 5 µm.

Figure 4 - video s11. Arp2/3 activity is required for JBL formation. Time-lapse video of JBL labelled with EGFP-UCHD, at around 32hpf, after 1h incubation with CK666 (200µM). Note the ectopic filopodia and stress fibers. scale bar: 5 µm.

suppl. Figure 3 - video s12. CK666 mediated JBL inhibition is reversible upon washout. Time-lapse video showing F-actin dynamics at the junctional ring, labeled with EGFP-UCHD during incubation with CK666 (200µM). Recording starts 30 minutes into the incubation. Blue arrowheads point to ectopic filopodia. scale bar 2µm.

suppl. Figure 3 - video s13. CK666 mediated JBL inhibition is reversible upon washout. Time-lapse video showing F-actin dynamics in the same junctional ring as in video s12 labeled with EGFP-UCHD, 90 min after start of washout. Red arrowheads point to reemerging JBL. scale bar 2µm.

Figure 4 - video s14. Arp2/3 activity is required for junction elongation. Time-lapse of a ZO1-tdTomato labeled junctional ring in the presence of DMSO (1%) (control) recorded over 60 minutes. scale bar: 10µm.

Figure 4 - video s15. Arp2/3 activity is required for junction elongation. Time-lapse of a ZO1-tdTomato labeled junctional ring after 1 hour incubation and in the presence of CK666 (200µM). scale bar: 10µm.

Figure 5 - video s16. Proximal and distal junctions merge at the end of JBL cycle. Time-lapse video showing of VE-cad-Venus during junctional merging over 90 seconds. Blue and red arrowheads point to the proximal and distal junction, respectively. The two junctions are gradually moving closer until they merge. scale bar: 2µm.

Figure 5 - video s17. Myl9 is enriched within the JBL. Time-lapse video showing Myl9a-GFP and mRuby2-UCHD localization during JBL formation during anastomosis of the PCeV of the zebrafish hindbrain at around 60 hpf. White dashed lines delineate the JBL region. Yellow and white arrowheads point to the proximal and distal junction, respectively. Myl9-GFP is enriched inside the lamellipodia and localizes at the distal junction at later time points. scale bar: 2 µm.

Figure 6 - video s18. Dynamic redistribution of Myl9 during JBL formation and junctional merging. Time-lapse video s18 of VE-cad-EGFP (Cdh5ΔC-EGFP) and Myl9b-mCherry (shown as “fire”-LUT) during junctional merging at four timepoints (0, 45, 90 and 135 seconds). Blue dashed lines confine the applied mask. Yellow and white arrowheads point to the proximal and distal junction, respectively. scale bars 2 µm.

suppl. Figure 4 - video s19. Myosin light-chain recruitment at the inter-junctional space during merging. Time-lapse of VEcad-EGFP (Cdh5ΔC-EGFP) and Myl9b-mCherry (shown as “fire”- LUT) during “double junction” state (video s19). scale bar: 2µm.

suppl. Figure 4 - video s20. Time-lapse video s20 of VE-cad-Venus and Myl9b-mCherry (shown as “fire”-LUT) showing increase of MLC in the inter-junctional space prior to proximodistal junction mergence. scale bar: 2µm.

suppl. Figure 4 - video s21. Time-laps video s21 showing VE-cad-EGFP (Cdh5ΔC-EGFP) and Myl9b-mCherry (shown as “fire”-LUT) showing recruitment of MLC between proximal and distal junction during “double junction” state. scale bar: 2µm.

suppl. Figure 4 - video s22. Time-laps video s22 showing VE-cad-EGFP (Cdh5ΔC-EGFP) and Myl9b-mCherry (shown as “fire”-LUT) showing recruitment of MLC between proximal and distal junction during “double junction” state. scale bar: 2µm.

Figure 7 - video s23. Junction elongation during DLAV formation requires actomyosin contractility (control). Time-lapse video showing elongation of endothelial cell-cell junctions (EGFP-UCHD) during DLAV formation at around 32 hpf (1% DMSO - control). scale bar: 10µm.

Figure 7 - video s24. Junction elongation during DLAV formation requires actomyosin contractility (Y-27632). Time-lapse video showing elongation of endothelial cell-cell junctions (EGFP-UCHD) during DLAV formation at around 32 hpf after 60-minute incubation with Y-27632 (45µM). scale bar: 10µm.

Figure 7 - video s25. Merging of proximal and distal junctions requires actomyosin contractility (control). Time-lapse video showing VE-cad-Venus labelled proximal and distal junction, during junctional merging (1% DMSO control) or Y-27632 (75 µM). Blue and yellow arrowheads are pointing distal and proximal junctions respectively. scale bar: 2µm.

Figure 7 - video s26. Merging of proximal and distal junctions requires actomyosin contractility (Y-27632). Time-lapse video showing VE-cad-Venus labelled proximal and distal junction, during junctional merging under ROCK inhibition (75µM Y-27632). Blue and yellow arrowheads are pointing distal and proximal junctions respectively. scale bar: 2µm.

Figure 8 - video s27. Animation depicting the molecular mechanisms of junction elongation by junction-based lamellipodia (JBL). JBL formation is initiated by Arp2/3 activation. The JBL is pushed forward by F-actin polymerization. At the distal end a new cell-cell junction is formed.

MyosinII is recruited to the interjunctional space. Actomyosin contraction merges the proximal and distal junctions resulting in an overall elongation of the junctional ring.

Note

This reviewed preprint has been updated to correct a corresponding author's email address, and include an author as corresponding author.

References

Aleström P., D'Angelo L., Midtlyng P. J., Schorderet D. F., Schulte-Merker S., Sohm F., Warner S. (2020) Zebrafish: Housing and husbandry recommendations. *Lab. Anim* **54**:213-224 https://doi.org/10.1177/0023677219869037 | PubMed

Alves N. G., Motawe Z. Y., Yuan S. Y., Breslin J. W. (2018) Endothelial Protrusions in Junctional Integrity and Barrier Function. *Curr. Top. Membr* **82**:93 https://doi.org/10.1016/bs.ctm.2018.08.006 | PubMed

Andrew D. J., Ewald A. J. (2010) Morphogenesis of epithelial tubes: Insights into tube formation, elongation, and elaboration. *Dev. Biol* **341**:34-55 https://doi.org/10.1016/j.ydbio.2009.09.024 | PubMed

Bagnat M., Cheung I. D., Mostov K. E., Stainier D. Y. R. (2007) Genetic control of single lumen formation in the zebrafish gut. *Nat. Cell Biol* **9**:954-960 https://doi.org/10.1038/ncb1621 | PubMed

Betz C., Lenard A., Belting H.-G., Affolter M. (2016) Cell behaviors and dynamics during angiogenesis. *Development (Cambridge)* **143**:2249-2260 https://doi.org/10.1242/dev.135616 | PubMed

Blaser H., Reichman-Fried M., Castanon I., Dumstrei K., Marlow F. L. L., Kawakami K., Solnica-Krezel L., Heisenberg C. P., Raz E. (2006) Migration of Zebrafish Primordial Germ Cells: A Role for Myosin Contraction and Cytoplasmic Flow. *Dev. Cell* **11**:613-627 https://doi.org/10.1016/j.devcel.2006.09.023 | PubMed

Blum Y., Belting H. G., Ellertsdóttir E., Herwig L., Lüders F., Affolter M. (2008) Complex cell rearrangements during intersegmental vessel sprouting and vessel fusion in the zebrafish embryo. *Dev. Biol* **316**:312-322 https://doi.org/10.1016/j.ydbio.2008.01.038 | PubMed

Cai D., Chen S. C., Prasad M., He L., Wang X., Choesmel-Cadamuro V., Sawyer J. K., Danuser G., Montell D. J. (2014) Mechanical feedback through E-cadherin promotes direction sensing during collective cell migration. *Cell* **157**:1146-1159 https://doi.org/10.1016/j.cell.2014.03.045 | PubMed

Campàs O., Noordstra I., Yap A. S. (2024) Adherens junctions as molecular regulators of emergent tissue mechanics. *Nat. Rev. Mol. Cell Biol* **25**:252-269 https://doi.org/10.1038/s41580-023-00688-7 | PubMed

Cao J., Schnittler H. (2019) Putting VE-cadherin into JAIL for junction remodeling. *J. Cell Sci* 132 https://doi.org/10.1242/jcs.222893 | PubMed

Cao J., Ehling M., März S., Seebach J., Tarbashevich K., Sixta T., Pitulescu M. E., Werner A. C., Flach B., Montanez E., *et al.* (2017) Polarized actin and VE-cadherin dynamics regulate junctional remodelling and cell migration during sprouting angiogenesis. *Nat. Commun* 8 https://doi.org/10.1038/s41467-017-02373-8 | PubMed

Dong B., Horie T., Denker E., Kusakabe T., Tsuda M., Smith W. C., Jiang D. (2009) Tube formation by complex cellular processes in Ciona intestinalis notochord. *Dev. Biol* **330**:237-249 https://doi.org/10.1016/j.ydbio.2009.03.015 | PubMed

Eberlein J., Herdt L., Helker C. S. M., Malchow J., Rittershaus A., Baumeister S. (2021) Molecular and cellular mechanisms of vascular development in zebrafish. *Life* 11 https://doi.org/10.3390/life11101088 | PubMed

Ellertsdóttir E., Lenard A., Blum Y., Krudewig A., Herwig L., Affolter M., Belting H. G. (2010) Vascular morphogenesis in the zebrafish embryo. *Dev. Biol* **341**:56-65 https://doi.org/10.1016/j.ydbio.2009.10.035 | PubMed

Fernandez-Gonzalez R., Simoes S. de M., Röper J. C., Eaton S., Zallen J. A. (2009) Myosin II dynamics are regulated by tension in intercalating cells. *Dev. Cell* **17**:736-743 https://doi.org/10.1016/j.devcel.2009.09.003 | PubMed

Franco C. A., Jones M. L., Bernabeu M. O., Vion A. C., Barbacena P., Fan J., Mathivet T., Fonseca C. G., Ragab A., Yamaguchi T. P., *et al.* (2016) Non-canonical wnt signalling modulates the endothelial shear stress flow sensor in vascular remodelling. *eLife* **5**:1-22 https://doi.org/10.7554/eLife.07727 | PubMed

Friedl P., Mayor R. (2017) Tuning collective cell migration by cell-cell junction regulation. *Cold Spring Harb. Perspect. Biol* **9**:1-18 https://doi.org/10.1101/cshperspect.a029199 | PubMed

Gebala V., Collins R., Geudens I., Phng L. K., Gerhardt H. (2016) Blood flow drives lumen formation by inverse membrane blebbing during angiogenesis in vivo. *Nat. Cell Biol* **18**:443-450 https://doi.org/10.1038/ncb3320 | PubMed

Gladysheva J., Evnukova E., Kondakova E., Kulakova M., Efremov V. (2021) Neurulation in the posterior region of zebrafish, Danio rerio embryos. *J. Morphol* **282**:1437-1454 https://doi.org/10.1002/jmor.21396 | PubMed

Henson J. H., Yeterian M., Weeks R. M., Medrano A. E., Brown B. L., Geist H. L., Pais M. D., Oldenbourg R., Shuster C. B. (2015) Arp2/3 complex inhibition radically alters lamellipodial actin architecture, suspended cell shape, and the cell spreading process. Molecular biology of the cell. https://doi.org/10.1091/mbc.E14-07-1244 | PubMed

Herwig L., Blum Y., Krudewig A., Ellertsdóttir E., Lenard A., Belting H. G., Affolter M. (2011) Distinct cellular mechanisms of blood vessel fusion in the zebrafish embryo. *Current Biology* **21**:1942-1948 https://doi.org/10.1016/j.cub.2011.10.016 | PubMed

Hetrick B., Han M. S., Helgeson L. A., Nolen B. J. (2013) Small molecules CK-666 and CK-869 inhibit actin-related protein 2/3 complex by blocking an activating conformational change. *Chem. Biol* **20**:701-712 https://doi.org/10.1016/j.chembiol.2013.03.019 | PubMed

Jakobsson L., Franco C. A., Bentley K., Collins R. T., Ponsioen B., Aspalter I. M., Rosewell I., Busse M., Thurston G., Medvinsky A., *et al.* (2010) Endothelial cells dynamically compete for the tip cell position during angiogenic sprouting. *Nat. Cell Biol* **12**:943-953 https://doi.org/10.1038/ncb2103 | PubMed

Jin S. W., Beis D., Mitchell T., Chen J. N., Stainier D. Y. R. (2005) Cellular and molecular analyses of vascular tube and lumen formation in zebrafish. *Development* **132**:5199-5209 https://doi.org/10.1242/dev.02087 | PubMed

Kipcke J. P., Odenthal-Schnittler M., Aldirawi M., Franz J., Bojovic V., Seebach J., Schnittler H. (2025) TNF-α induces VE-cadherin-dependent gap/JAIL cycling through an intermediate state essential for neutrophil transmigration. *Front. Immunol* 16 https://doi.org/10.3389/fimmu.2025.1665264 | PubMed

Lagendijk A. K., Gomez G. A., Baek S., Hesselson D., Hughes W. E., Paterson S., Conway D. E., Belting H. G., Affolter M., Smith K. A., *et al.* (2017) Live imaging molecular changes in junctional tension upon VE-cadherin in zebrafish. *Nat. Commun* 8 https://doi.org/10.1038/s41467-017-01325-6 | PubMed

Lancino M., Majello S., Herbert S., De Chaumont F., Tinevez J. Y., Olivo-Marin J. C., Herbomel P., Schmidt A. (2018) Anisotropic organization of circumferential actomyosin characterizes hematopoietic stem cells emergence in the zebrafish. *eLife* **7**:1-36 https://doi.org/10.7554/eLife.37355 | PubMed

Lecuit T., Lenne P. F., Munro E. (2011) Force generation, transmission, and integration during cell and tissue morphogenesis. *Annu. Rev. Cell Dev. Biol* **27**:157-184 https://doi.org/10.1146/annurev-cellbio-100109-104027 | PubMed

Lenard A., Ellertsdóttir E., Herwig L., Krudewig A., Sauteur L., Belting H. G., Affolter M. (2013) In vivo analysis reveals a highly stereotypic morphogenetic pathway of vascular anastomosis. *Dev. Cell* **25**:492-506 https://doi.org/10.1016/j.devcel.2013.05.010 | PubMed

Lowery L. A., Sive H. (2005) Initial formation of zebrafish brain ventricles occurs independently of circulation and requires the nagie oko and snakehead/atp1a1a.1 gene products. *Development* **132**:2057-2067 https://doi.org/10.1242/dev.01791 | PubMed

Maître J. L., Heisenberg C. P. (2013) Three functions of cadherins in cell adhesion. *Current Biology* **23**:626-633 https://doi.org/10.1016/j.cub.2013.06.019 | PubMed

Malchow J., Eberlein J., Li W., Hogan B. M., Okuda K. S., Helker C. S. M. (2024) Neural progenitor-derived Apelin controls tip cell behavior and vascular patterning. *Sci. Adv* **10**:1174 https://doi.org/10.1126/sciadv.adk1174 | PubMed

Martinelli R., Kamei M., Sage P. T., Massol R., Varghese L., Sciuto T., Toporsian M., Dvorak A. M., Kirchhausen T., Springer T. A., *et al.* (2013) Release of cellular tension signals self-restorative ventral lamellipodia to heal barrier micro-wounds. *Journal of Cell Biology* **201**:449-465 https://doi.org/10.1083/jcb.201209077 | PubMed

Mayor R., Etienne-Manneville S. (2016) The front and rear of collective cell migration. *Nat. Rev. Mol. Cell Biol* **17**:97-109 https://doi.org/10.1038/nrm.2015.14 | PubMed

Munjal A., Philippe J. M., Munro E., Lecuit T. (2015) A self-organized biomechanical network drives shape changes during tissue morphogenesis. *Nature* **524**:351-355 https://doi.org/10.1038/nature14603 | PubMed

Munson C., Huisken J., Bit-Avragim N., Kuo T., Dong P. D., Ober E. A., Verkade H., Abdelilah-Seyfried S., Stainier D. Y. R. (2008) Regulation of neurocoel morphogenesis by Pard6γb. *Dev. Biol* **324**:41-54 https://doi.org/10.1016/j.ydbio.2008.08.033 | PubMed

Navis A., Bagnat M. (2015) Developing pressures: FLUID forces driving morphogenesis. *Curr. Opin. Genet. Dev* **32**:24-30 https://doi.org/10.1016/j.gde.2015.01.010 | PubMed

Noordstra I., Hermoso M. D., Schimmel L., Bonfim-Melo A., Currin-Ross D., Duong C. N., Kalappurakkal J. M., Morris R. G., Vestweber D., Mayor S., *et al.* (2023) An E-cadherin-actin clutch translates the mechanical force of cortical flow for cell-cell contact to inhibit epithelial cell locomotion. *Dev. Cell* **58**:1748-1763.e6 https://doi.org/10.1016/j.devcel.2023.06.011 | PubMed

Paatero I., Sauteur L., Lee M., Lagendijk A. K., Heutschi D., Wiesner C., Guzmán C., Bieli D., Hogan B. M., Affolter M., *et al.* (2018) Junction-based lamellipodia drive endothelial cell rearrangements in vivo via a VE-cadherin-F-actin based oscillatory cell-cell interaction. *Nat. Commun* 9 https://doi.org/10.1038/s41467-018-05851-9 | PubMed

Padrick S. B., Doolittle L. K., Brautigam C. A., King D. S., Rosen M. K. (2011) Arp2/3 complex is bound and activated by two WASP proteins. *Proc. Natl. Acad. Sci. U. S. A* **108**:E472-E479 https://doi.org/10.1073/pnas.1100236108 | PubMed

Phng L.-K. (2018) Endothelial Cell Dynamics during Blood Vessel Morphogenesis. In: Hirata H., Iida A. (Eds). *Zebrafish, Medaka, and Other Small Fishes* Springer. pp. 17-35 https://doi.org/10.1007/978-981-13-1879-5_2

Phng L. K., Belting H. G. (2021) Endothelial cell mechanics and blood flow forces in vascular morphogenesis. *Semin. Cell Dev. Biol* **120**:32-43 https://doi.org/10.1016/j.semcdb.2021.06.005 | PubMed

Sauteur L., Krudewig A., Herwig L., Ehrenfeuchter N., Lenard A., Affolter M., Belting H. G. (2014) Cdh5/VE-cadherin promotes endothelial cell interface elongation via cortical actin polymerization during angiogenic sprouting. *Cell Rep* **9**:504-513 https://doi.org/10.1016/j.celrep.2014.09.024 | PubMed

Schoofs H., Daubel N., Schnabellehner S., Grönloh M. L. B., Palacios Martínez S., Halme A., Marks A. M., Jeansson M., Barcos S., Benedito R., *et al.* (2025) Dynamic cytoskeletal regulation of cell shape supports resilience of lymphatic endothelium. *Nature* **641**:465-475 https://doi.org/10.1038/s41586-025-08724-6 | PubMed

Schuermann A., Helker C. S. M., Herzog W. (2014) Angiogenesis in zebrafish. *Semin. Cell Dev. Biol* **31**:106-114 https://doi.org/10.1016/j.semcdb.2014.04.037 | PubMed

Seebach J., Klusmeier N., Schnittler H. (2021) Autoregulatory "Multitasking" at Endothelial Cell Junctions by Junction-Associated Intermittent Lamellipodia Controls Barrier Properties. *Front. Physiol* 11 https://doi.org/10.3389/fphys.2020.586921 | PubMed

Strilić B., Kučera T., Eglinger J., Hughes M. R., McNagny K. M., Tsukita S., Dejana E., Ferrara N., Lammert E. (2009) The Molecular Basis of Vascular Lumen Formation in the Developing Mouse Aorta. *Dev. Cell* **17**:505-515 https://doi.org/10.1016/j.devcel.2009.08.011 | PubMed

Taha A. A., Schnittler H. J. (2014) Dynamics between actin and the VE-cadherin/ catenin complex: Novel aspects of the ARP2/3 complex in regulation of endothelial junctions. *Cell Adh. Migr* **8**:125-135 https://doi.org/10.4161/cam.28243 | PubMed

Taha A. A., Taha M., Seebach J., Schnittler H. J. (2014) ARP2/3-mediated junction-associated lamellipodia control VE-cadherin-based cell junction dynamics and maintain monolayer integrity. *Mol. Biol. Cell* **25**:245-256 https://doi.org/10.1091/mbc.E13-07-0404 | PubMed

Uehata M., Ishizaki T., Satoh H., Ono T., Kawahara T., Morishita T., Tamakawa H., Yamagami K., Inui J., Maekawa M., *et al.* (1997) Calcium sensitization of smooth muscle mediated by a Rho-associated protein kinase in hypertension. *Nature* **389**:990-994 https://doi.org/10.1038/40187 | PubMed

Westerfield M. (2007) *The Zebrafish Book. A Guide for the Laboratory Use of Zebrafish (Danio rerio)* (5th) Eugene: University of Oregon Press.

Yin J., Schellinx N., Maggi L., Gundel K., Wiesner C., Kotini M. P., Lee M., Phng L.-K., Belting H.-G., Affolter M. (2024) Initiation of lumen formation from junctions via differential actomyosin contractility regulated by dynamic recruitment of Rasip1. *Nat. Commun* **15**:9714 https://doi.org/10.1038/s41467-024-54143-y | PubMed

Zeeb M., Strilić B., Lammert E. (2010) Resolving cell-cell junctions: Lumen formation in blood vessels. *Curr. Opin. Cell Biol* **22**:626-632 https://doi.org/10.1016/j.ceb.2010.07.003 | PubMed

Peer reviews

Reviewer #1 (Public review):

[Editors' note: this version has been assessed by the Reviewing Editor without further input from the original reviewers. The authors have addressed the comments raised in the previous round of review.]

Original review:

Summary:

Lumen formation is a fundamental morphogenetic event essential for the function of all tubular organs, notably the vertebrate vascular network, where continuous and patent conduits ensure blood flow and tissue perfusion. The mechanisms by which endothelial cells organize to create and maintain luminal space have historically been categorized into two broad strategies: cell shape changes, which involve alterations in apical-basal polarity and cytoskeletal architecture, and cell rearrangements, wherein intercellular junctions and positional relationships are remodeled to form uninterrupted conduits. The study presented here focuses on the latter process, highlighting a unique morphogenetic module, junction-based lamellipodia (JBL), as the driver for endothelial rearrangements.

Strengths:

The key mechanistic insight from this work is the requirement of the Arp2/3 complex, the classical nucleator of branched actin filament networks, for JBL protrusion. This implicates Arp2/3-mediated actin polymerization in pushing force generation, enabling plasma membrane advancement at junctional sites. The dependence on Arp2/3 positions JBL within the family of lamellipodia-like structures, but the junctional origin and function distinguish them from canonical, leading-edge lamellipodia seen in cell migration.

Weaknesses:

The study primarily presents descriptive observations and includes limited quantitative analyses or genetic modifications. Molecular mechanisms are typically interrogated through the use of pharmacological inhibitors rather than genetic approaches. Furthermore, the precise semantic distinction between JAIL and JBL requires additional clarification, as current evidence suggests their biological relevance may substantially overlap.

https://doi.org/10.7554/eLife.109264.2.sa3

Reviewer #2 (Public review):

Original review:

Summary:

In Maggi et al., the authors investigated the mechanisms that regulate the dynamics of a specialized junctional structure called junction-based lamellipodia (JBL), which they have previously identified during multicellular vascular tube formation in the zebrafish. They identified the Arp2/3 complex to dynamically localize at expanding JBLs and showed that the chemical inhibition of Arp2/3 activity slowed junctional elongation. The authors therefore concluded that actin polymerization at JBLs pushes the distal junction forward to expand the JBL. They further revealed the accumulation of Myl9a/Myl9b (marker for MLC) at the junctional pole, at interjunctional regions, suggesting that contractile activity drives the merging of proximal and distal junctions. Indeed, chemical inhibition of ROCK activity decreased junctional mergence. With these new findings, the authors added new molecular and cellular details into the previously proposed clutch mechanism by proposing that Arp2/3-dependent actin polymerization provides pushing forces while actomyosin contractility drives the merging of proximal and distal junctions, explaining the oscillatory protrusive nature of JBLs.

Strengths:

The authors provide detailed analyses of endothelial cell-cell dynamics through time-lapse imaging of junctional and cytoskeletal components at subcellular resolution. The use of zebrafish as an animal model system is invaluable in identifying novel mechanisms that explain the organizing principles of how blood vessels are formed. The data is well presented, and the manuscript is easy to read.

Weaknesses:

While the data generally support the conclusions reached, some aspects can be strengthened. For the untrained eye, it is unclear where the proximal and distal junctions are in some images, and so it is difficult to follow their dynamics (especially in experiments where Cdh5 is used as the junctional marker). Images would benefit from clear annotation of the two junctions. All perturbation experiments were done using chemical inhibitors; this can be further supported by genetic perturbations.

https://doi.org/10.7554/eLife.109264.2.sa2

Reviewer #3 (Public review):

Original review:

The paper by Maggi et al. builds on earlier work by the team (Paatero et al., 2018) on oriented junction-based lamellipodia (JBL). They validate the role of JBLs in guiding endothelial cell rearrangements and utilise high-resolution time-lapse imaging of novel transgenic strains to visualise the formation of distal junctions and their subsequent fusion with proximal

junctions. Through functional analyses of Arp2/3 and actomyosin contractility, the study identifies JBLs as localized mechanical hubs, where protrusive forces drive distal junction formation, and actomyosin contractility brings together the distal and proximal junctions. This forward movement provides a unique directionality which would contribute to proper lumen formation, EC orientation, and vessel stability during these early stages of vessel development.

Time-lapse live imaging of VEC, ZO-1, and actin reveals that VEC and ZO-1 are initially deposited at the distal junction, while actin primarily localizes to the region between the proximal and distal sites. Using a photoconvertible Cdh5-mClav2 transgenic line, the origin of the VEC aggregates was examined. This convincingly shows that VE-cadherin was derived from pools outside the proximal junctions. However, in addition to de novo VEC derived from within the photoconverted cell, could some VEC also be contributed by the neighbouring endothelial cell to which the JBL is connected?

As seen for JAILs in cultured ECs, the study reveals that Arp2/3 is enhanced when JBLs form by live imaging of Arpc1b-Venus in conjunction with ZO-1 and actin. Therefore Arp2/3 likely contributes to the initial formation of the distal junction in the lamellopodium.

Inhibiting Arp2/3 with CK666 prevents JBL formation, and filopodia form instead of lamellopodia. This loss of JBLs leads to impaired EC rearrangements.

Is the effect of CK666 treatment reversible? Since only a short (30 min) treatment is used, the overall effect on the embryo would be minimal, and thus washing out CK666 might lead to JBL formation and normalized rearrangements, which would further support the role of Arp2/3.

From the images in Figure 4d it appears that ZO-1 levels are increased in the ring after CK666 treatment. Has this been investigated, and could this overall stabilization of adhesion proteins further prevent elongation of the ring?

To explore how the distal and proximal junctions merge, imaging of spatiotemporal imaging of Myl9 and VEC is conducted. It indicates that Myl9 is localized at the interjunctional fusion site prior to fusion. This suggests pulling forces are at play to merge the junctions, and indeed Y 27632 treatment reduces or blocks the merging of these junctions.

For this experiment, a truncated version of VEC was use,d which lacks the cytoplasmic domain. Why have the authors chosen to image this line, since lacking the cytoplasmic domain could also impair the efficiency of tension on VEC at both junction sites? This is as described in the discussion (lines 328-332).

Since the time-lapse movies involve high-speed imaging of rather small structures, it is understandable that these are difficult to interpret. Adding labels to indicate certain structures or proteins at essential timepoints in the movies would help the readers understand these.

https://doi.org/10.7554/eLife.109264.2.sa1

Author response:

The following is the authors' response to the original reviews.

> ***Public Reviews:***
>
> ***Reviewer #1 (Public review):***
>
> *Summary:*

> *Lumen formation is a fundamental morphogenetic event essential for the function of all tubular organs, notably the vertebrate vascular network, where continuous and patent conduits ensure blood flow and tissue perfusion. The mechanisms by which endothelial cells organize to create and maintain luminal space have historically been categorized into two broad strategies: cell shape changes, which involve alterations in apical-basal polarity and cytoskeletal architecture, and cell rearrangements, wherein intercellular junctions and positional relationships are remodeled to form uninterrupted conduits. The study presented here focuses on the latter process, highlighting a unique morphogenetic module, junction-based lamellipodia (JBL), as the driver for endothelial rearrangements.*
>
> *Strengths:*
>
> *The key mechanistic insight from this work is the requirement of the Arp2/3 complex, the classical nucleator of branched actin filament networks, for JBL protrusion. This implicates Arp2/3-mediated actin polymerization in pushing force generation, enabling plasma membrane advancement at junctional sites. The dependence on Arp2/3 positions JBL within the family of lamellipodia-like structures, but the junctional origin and function distinguish them from canonical, leading-edge lamellipodia seen in cell migration.*
>
> *Weaknesses:*
>
> *The study primarily presents descriptive observations and includes limited quantitative analyses or genetic modifications. Molecular mechanisms are typically interrogated through the use of pharmacological inhibitors rather than genetic approaches. Furthermore, the precise semantic distinction between JAIL and JBL requires additional clarification, as current evidence suggests their biological relevance may substantially overlap.*

We have previously analyzed the effects of different *ve-cadherin* (*cdh5*) mutant alleles on EC rearrangements (Paatero et al., 2018; Sauteur et al., 2014).These mutants show complex defects (e.g. hypersprouting, reduced contact inhibition during anastomosis) in EC behavior early in vascular tube formation. We find that analysis of JBL dynamics and function is very difficult in such situations. The use of small molecule inhibitors allows acute interventions within a defined time-window and to avoid pleiotropic effects of genetic ablations. We have expanded our discussion on the distinction between JAIL and JBL and hope that this will clarify why – in our opinion – these terms should be used differentially in different cell biological contexts (see below and lines 348-374 in the manuscript).

> ***Reviewer #2 (Public review):***
>
> *Summary:*
>
> *In Maggi et al., the authors investigated the mechanisms that regulate the dynamics of a specialized junctional structure called junction-based lamellipodia (JBL), which they have previously identified during multicellular vascular tube formation in the zebrafish. They identified the Arp2/3 complex to dynamically localize at expanding JBLs and showed that the chemical inhibition of Arp2/3 activity slowed junctional elongation. The authors therefore concluded that actin polymerization at JBLs pushes the distal junction forward to expand the JBL. They further revealed the accumulation of Myl9a/Myl9b (marker for MLC) at the junctional pole, at interjunctional regions, suggesting that contractile activity drives the merging of proximal and distal junctions. Indeed, chemical inhibition of ROCK activity decreased junctional mergence. With these new findings, the authors added new molecular and cellular details into the previously proposed clutch mechanism by proposing that Arp2/3-dependent actin polymerization provides pushing forces while*

> *actomyosin contractility drives the merging of proximal and distal junctions, explaining the oscillatory protrusive nature of JBLs.*
>
> *Strengths:*
>
> *The authors provide detailed analyses of endothelial cell-cell dynamics through time-lapse imaging of junctional and cytoskeletal components at subcellular resolution. The use of zebrafish as an animal model system is invaluable in identifying novel mechanisms that explain the organizing principles of how blood vessels are formed. The data is well presented, and the manuscript is easy to read.*
>
> *Weaknesses:*
>
> *While the data generally support the conclusions reached, some aspects can be strengthened. For the untrained eye, it is unclear where the proximal and distal junctions are in some images, and so it is difficult to follow their dynamics (especially in experiments where Cdh5 is used as the junctional marker). Images would benefit from clear annotation of the two junctions. All perturbation experiments were done using chemical inhibitors; this can be further supported by genetic perturbations.*

We have added annotations to several figures and paid particular attention to the proximal and distal junctions.

We have previously analyzed the effects of different *ve-cadherin* (*cdh5*) mutant alleles on EC rearrangements (Paatero et al., 2018; Sauteur et al., 2014). These mutants show complex defects (e.g. hypersprouting, reduced contact inhibition during anastomosis) in EC behavior early in vascular tube formation. We find that analysis of JBL dynamics and function is very difficult in such situations. The use of small inhibitors allows acute interventions within a defined time-window and to avoid pleiotropic effects of genetic ablations.

> ***Reviewer #3 (Public review):***
>
> *The paper by Maggi et al. builds on earlier work by the team (Paatero et al., 2018) on oriented junction-based lamellipodia (JBL). They validate the role of JBLs in guiding endothelial cell rearrangements and utilise high-resolution time-lapse imaging of novel transgenic strains to visualise the formation of distal junctions and their subsequent fusion with proximal junctions. Through functional analyses of Arp2/3 and actomyosin contractility, the study identifies JBLs as localized mechanical hubs, where protrusive forces drive distal junction formation, and actomyosin contractility brings together the distal and proximal junctions. This forward movement provides a unique directionality which would contribute to proper lumen formation, EC orientation, and vessel stability during these early stages of vessel development.*
>
> *Time-lapse live imaging of VEC, ZO-1, and actin reveals that VEC and ZO-1 are initially deposited at the distal junction, while actin primarily localizes to the region between the proximal and distal sites. Using a photoconvertible Cdh5-mClav2 transgenic line, the origin of the VEC aggregates was examined. This convincingly shows that VE-cadherin was derived from pools outside the proximal junctions. However, in addition to de novo VEC derived from within the photoconverted cell, could some VEC also be contributed by the neighbouring endothelial cell to which the JBL is connected?*

Yes, the green (non-converted) VE-cadherin can indeed originate from either of the two cells. The main point we want to make, based on our observations, is that the red (converted) VE-cadherin from the proximal junction (as defined by the ROI) does not contribute to the distal junction.

> *As seen for JAILs in cultured ECs, the study reveals that Arp2/3 is enhanced when JBLs form by live imaging of Arpc1b-Venus in conjunction with ZO-1 and actin. Therefore Arp2/3 likely contributes to the initial formation of the distal junction in the lamellopodium.*
>
> *Inhibiting Arp2/3 with CK666 prevents JBL formation, and filopodia form instead of lamellopodia. This loss of JBLs leads to impaired EC rearrangements.*
>
> *Is the effect of CK666 treatment reversible? Since only a short (30 min) treatment is used, the overall effect on the embryo would be minimal, and thus washing out CK666 might lead to JBL formation and normalized rearrangements, which would further support the role of Arp2/3.*

We have performed washout experiments and find that the ectopic filopodia disappear when the inhibitor is removed. This experiment is shown in supplementary Figure 3 and supplementary Movies 12 and 13.

> *From the images in Figure 4d it appears that ZO-1 levels are increased in the ring after CK666 treatment. Has this been investigated, and could this overall stabilization of adhesion proteins further prevent elongation of the ring?*

This is an interesting thought and we haven take a closer look. There is quite a bit of sample-to-sample variation in the ZO1 signal. The quantification (Author response image 1) indicates that there is no increase in the CK666 treated embryos on average.

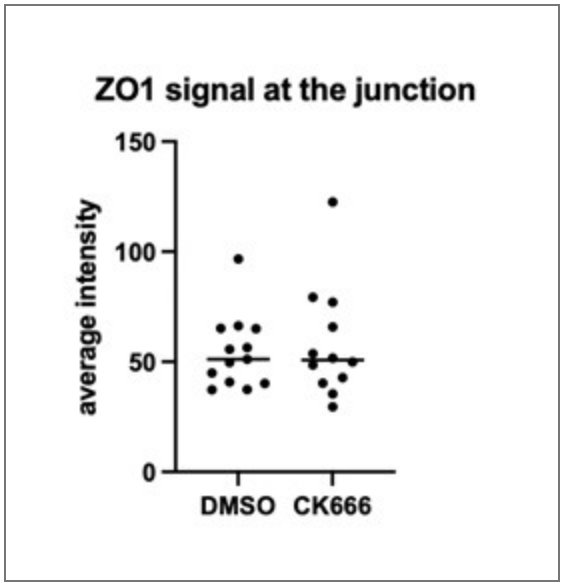

Author response image 1.

> *To explore how the distal and proximal junctions merge, imaging of spatiotemporal imaging of Myl9 and VEC is conducted. It indicates that Myl9 is localized at the interjunctional fusion site prior to fusion. This suggests pulling forces are at play to merge the junctions, and indeed Y 27632 treatment reduces or blocks the merging of these junctions.*

> *For this experiment, a truncated version of VEC was use,d which lacks the cytoplasmic domain. Why have the authors chosen to image this line, since lacking the cytoplasmic domain could also impair the efficiency of tension on VEC at both junction sites? This is as described in the discussion (lines 328-332).*

This line was used because it labels the entire JBL protrusion more clearly. We have also included an example using the VE-cad-Venus line (supplementary Figure 4b), which shows a Myl-Cherry pattern consistent with the other examples.

> *Since the time-lapse movies involve high-speed imaging of rather small structures, it is understandable that these are difficult to interpret. Adding labels to indicate certain structures or proteins at essential timepoints in the movies would help the readers understand these.*

We have added annotations and labels to all movies. We have also improved annotations in several figures (i.e. Figs. 1, 2, 5, 6 and 7)

> ***Recommendations for the authors:***
>
> ***Reviewing Editor Comments:***
>
> *Overall, the reviewers are supportive of the manuscript but identify a number of areas where the clarity of the presented data could be improved, and further quantification could be provided to strengthen your conclusions. We would encourage you to address these minor concerns as best you can and to consider the recommendations of all three reviewers when deciding how to revise your manuscript.*
>
> ***Reviewer #1 (Recommendations for the authors):***
>
> *Lumen formation is a fundamental morphogenetic event essential for the function of all tubular organs, notably the vertebrate vascular network, where continuous and patent conduits ensure blood flow and tissue perfusion. The mechanisms by which endothelial cells organize to create and maintain luminal space have historically been categorized into two broad strategies: cell shape changes, which involve alterations in apical-basal polarity and cytoskeletal architecture, and cell rearrangements, wherein intercellular junctions and positional relationships are remodeled to form uninterrupted conduits. The study presented here focuses on the latter process, highlighting a unique morphogenetic module, junction-based lamellipodia (JBL), as the driver for endothelial rearrangements.*
>
> *JBL are described as oscillating membrane protrusions emerging at endothelial junctions, operating in a ratchet-like manner to mediate convergent cell movements. This ratchet mechanism allows endothelial cells to approach each other, thereby aligning and joining local luminal segments into a continuous vascular structure. The study employs in vivo high-resolution time-lapse imaging, a technically demanding method that captures spatiotemporal dynamics of cytoskeletal and adhesion complexes during JBL activity with unprecedented detail.*
>
> *The key mechanistic insight from this work is the requirement of the Arp2/3 complex, the classical nucleator of branched actin filament networks, for JBL protrusion. This implicates Arp2/3-mediated actin polymerization in pushing force generation, enabling plasma membrane advancement at junctional sites. The dependence on Arp2/3 positions JBL within the family of lamellipodia-like structures, but the junctional origin and function distinguish them from canonical, leading-edge lamellipodia seen in cell migration.*

> *An intriguing observation is that a novel junction arises at the distal pole of a JBL. This distal junction is formed from a pool of VE-cadherin that is spatially redistributed from regions outside the initial JBL domain. The distal junction then merges with the proximal junction through a process dependent on actomyosin contractility, as was judged by Myl9 recruitment.*
>
> *The alternation between pushing forces (Arp2/3-dependent JBL protrusion) and pulling forces (actomyosin-driven junction fusion) defines JBL as a bidirectional mechanical module. Inhibition of actomyosin prevents merging of proximal and distal junctions, thereby stalling lumen continuity. This two-phase system, actin-based extension followed by actomyosin-mediated constriction, ensures both elongation and maturation of endothelial arrangements, ultimately securing vascular patency.*
>
> *This manuscript represents a robust and thoughtfully executed study that advances our understanding of lumen formation during vascular development. The overarching conclusions are well substantiated, and the results section provides a clear and detailed exposition of the key findings. I appreciate the explanatory movie at the end. Nevertheless, I offer several remarks for further improvement:*
>
> *(1) The fluorescent images presented are visually compelling, yet lack quantitative analysis in the initial figure. Although quantification is included in Figure 3, it is advisable to incorporate this analysis into Figure 1 as well. Early presentation of quantification will help the reader to appreciate the impact and significance of the findings from the outset.*

We appreciate the reviewer's suggestion and have now added line graphs to measure the spatiotemporal intensities of the Utrophin and ZO-1 reporters in Figure 1b. These measurements demonstrate the sequence of F-actin protrusion and subsequent junctional movement. In Figure 1a, we have added a double-headed arrow which shows the overall movement of the junction towards the dorsal side of the forming DLAV.

> *(2) For the fluorescence images, further quantitative analysis of membrane overlap, either in terms of width or pixel overlap, would enhance the rigor of the study. Temporal quantification of overlap may provide valuable insights into the stability and reproducibility of the process across experimental replicates.*

JBL are quite heterogenous with respect to size, shape and dynamics, which makes quantifications of membrane overlap (JBL size) across experimental replicates difficult. We have published some quantifications on JBL orientation and oscillation in our previous paper (Paatero et al., 2018, Nat. comm. Figures 1 and 2), which are in agreement with our current study.

> *(3) When referencing the role of Arp2/3, the authors employ an ArpC1b transgenic fish. The results section should thus specifically address the involvement of ArpC1b, rather than generalizing to Arp2/3. In the discussion, it would be appropriate to speculate on the potential involvement of the complete Arp2/3 complex. Notably, the use of CK is acknowledged as a broadly accepted inhibitor of actin polymerization.*

As ArpC1b is a subunit of an active Arp2/3 complex (Padrick et al., 2011), we have used an ArpC1b-Venus as a readout for Arp2/3 localization. The construct has been validated before in cell culture (Law et al., 2021) as well as in zebrafish (Malchow et al., 2024) and the spatiotemporal distribution of the reporter shown to be consistent with Arp2/3 complex. We are stating this in the results section (lines 173-178) and subsequently use the term Arp2/3 to facilitate reading of the text. In the corresponding figure legends, we are maintaining the term ArpC1b. CK666 interferes with the dimerization of Arp2 and Arp3 subunits and thus prevents activity of the Arp2/3 complex.

> *(4) The discussion regarding JAIL versus JBL involvement remains challenging to interpret. If JAIL structures arise from the loss of cell-cell contacts, both JAIL and JBL resemble membrane protrusions and are likely governed by similar molecular mechanisms, predominantly actin polymerization and Arp2/3 activity, with probable contribution from Rac1 signaling. The precise semantic distinction between JAIL and JBL warrants further clarification, as their biological relevance may be overlapping.*

We agree with the reviewer. Below we outline the reasons why lamellipodial protrusions that emanate from cell-cell junctions should not be indiscriminately called JAIL, but that JAIL and JBL constitute different cellular activities acting in different tissue contexts. We have modified the text in the Discussion (lines 348-374).

(1) JAIL have originally been described in cell culture experiments (Abu-Taha et al., 2014). According to this and subsequent papers by the same group, local dissolution of endothelial adherens junctions (i.e. downregulation of VE-cadherin) triggers the formation of lamellipodia-like structures. These protrusions eventually retract, followed by the reestablishment of EC junctions.

(2) In our in vivo studies, we observed lamellipodial protrusions during endothelial cell rearrangements, and we call these structures JBL (Paatero et al., 2018). While JBL appear very similar to JAIL in general (i.e. regulation by Arp2/3 and its localization), we also observe two critical differences. For one, JBL form while maintaining the original (proximal) junction. Moreover, a distal junction is formed at the front edge of the JBL, leading to a “double junction” configuration. In our current manuscript, we have examined the role of actomyosin contractility and find that it correlates with and is required for the merging of proximal and distal junctions during JBL cycles. These observations indicates that the proximal and distal junctions are essential components of JBL function during endothelial cell elongation and rearrangements. These salient and distinct features prompted us to adopt the term junction-based-lamellipodia (JBL), in order to differentiate them from JAIL.

(3) We like to argue that JAIL and JBL represent similar but different lamellipodia-like protrusions. JAILs are associated with the maintenance of endothelial integrity, and control permeability and trans-endothelial cell migration, as has been suggested by several publications (Cao et al., 2017; Kipcke et al., 2025; Seebach et al., 2021; Taha et al., 2014). In contrast, JBL drive cell rearrangements, by step-wise elongation of cell junctions leading to convergent cell movements.

(4) Although JAIL have also been implicated in endothelial cell migration (Cao and Schnittler, 2019; Cao et al., 2017; Seebach et al., 2021), neither junctional patterns nor junctional dynamics have been analyzed in this context. We therefore propose that JAIL and JBL are actin-based protrusions forming at endothelial cell-cell junctions, but act in different contexts to provide cell motility (JBL) or endothelial integrity (JAIL).

> *(5) Some of the quantification plots, specifically in figures 5d and 6c, do not display significant differences or distribution patterns. It would be beneficial to revise these graphs to clearly represent statistical significance and underlying data distributions.*

Because of the spatiotemporal heterogeneity, it is difficult to perform statistical quantifications across samples. In Figure 5c/d, we have imaged/analyzed myl9-EGFP in a mosaic situation, in which only one of interacting cells expresses high levels of myl9-EGFP. This is a rare situation and we managed to image only this example. Nevertheless, it is consistent with our other expression data of myl9-reporters and also with our previous photoconversion experiments using photoconvertible UCHD (Paatero et al., 2018, Figure 4), which shows that actin-rich JBL form at the front end of the endothelial cell in the direction of junction elongation. In Figure 5d, we have quantified the average intensity of GFP signal

within the region of interest. The newly added error bars indicate the standard deviation between pixel intensities within the ROI.

In Figure 6c, we have analyzed the Myl9b-mCherry intensities and find that it is redistributed during a JBL cycle. The spatial distribution is evident from the heat-map and we have not included a standard deviation. Myl9b-mCherry levels are very heterogenous and is not possible to quantify intensities across samples. We have, however, included four more examples of Myl9b-mCherry distribution in Supplementary Figure 4. The patterns observed in these samples are consistent with those in Figure 6.

> *(6) The observation of myosin recruitment does not inherently imply a concomitant increase in actomyosin contractile activity. The inclusion of phospho-MLC staining would considerably strengthen the evidence for enhanced actomyosin activity.*

This is a good suggestion and we have extensively tried different anti-P-Myl antibodies (and protocols), but did not get them to work reliably on zebrafish embryos. We therefore rely on published work that has established the correlation between the recruitment of myosin light chain and increased actomyosin tension (Fernandez-Gonzalez et al., 2009; Munjal et al., 2015).

> ***Reviewer #2 (Recommendations for the authors):***
>
> *(1) Figure 1a is not described/mentioned in the Results.*

The have corrected this (lines 102-108). We have also added measurements to better present the different dynamics of F-actin (UCHD) and ZO1 within the JBL and the relative endothelial cell movements (see Figure 1b), as suggested by reviewer#1.

> *(2) In Figure 3a, the authors claim that Arp2/3 is deposited at the distal side of the junction ring. While it is clear where the proximal junction is (ZO1-rich), the distal junction is less so (hardly any ZO1). It is therefore difficult to agree based on this time-lapse imaging that Arpc1b-Venus is at the distal junction. Can the authors please include panels showing merged channels and annotate where the proximal and distal junctions are?*

The activation of the Arp2/3 complex and the formation of the distal junction are sequential events. We see that ArpC1b oscillates with an accumulation at the onset and during JBL protrusion. In contrast, the distal junction is formed when the protrusive activity has been stopped. One caveat of the analysis shown in Figure 3a is that our ZO1 reporters label the distal junction only very weakly – this is in particular the case for the ZO1-tdTomato knock-in. The distal junction is better visible in VE-cadherin and UCHD reporters, as shown in Figures 5 to 7.

> *(3) In Figures 3b and c, it is also difficult to distinguish proximal and distal junctions in these images. Please mark the boundaries in the image panels (Figure 3b) and indicate on the x-axis where the proximal and distal junctions are (Figure 3c).*

In Figure 3b, we show ArpC1b-Venus and mRuby-UCHD side-by-side. This Figure demonstrates that the Arp2/3 complex maintains its position at the front of the JBL during the protrusive phase (always distal to the UCHD signal). The imaging is done at very short intervals (1/30sec), which makes it difficult to follow entire oscillations due to photo-bleaching of the ArpC1b reporter.

> *(4) The treatment of CK666 resulted in perturbed localization of Arpc1b-Venus. Therefore, the inhibition of junctional elongation can also be explained by the mislocalization of Arp2/3, rather than the inhibition of Arp2/3 activity at the junctions. Can the authors discuss this or perform another experiment that is more specific to manipulating Arp2/3 activity?*

CK666 is a well-established inhibitor of Arp2/3. Structural and functional analyses have shown that CK666 interferes with the interaction between Arp2 and Arp3, thereby preventing the activation of the complex (Hetrick et al., 2013; Padrick et al., 2011). We therefore conclude that the phenotypes we observe in CK666 treatment are due to Arp2/3 inhibition.

It is possible that CK666 prevents ArpC1b binding to the Arp2/3 complex. However, published work suggests that ArpC1b can bind to Arp2/3 also in its inactive state (Chou et al., 2022). Thus, we can only speculate why we lose localization ArpC1b under CK666. We prefer not to do so.

> *(5) In Figures 5d and 6c, is the quantification of Myl9 intensity of one cell only? If so, can the authors show the dynamics of average Myl9 intensity i) between forwarding and non-forwarding JBL poles and ii) as the proximal and distal junctions merge several endothelial cells?*

Figure 5c/d depicts two interacting cells, expressing different levels of Myl9a-EGFP. This is a rare experimental situation and we managed to image only this example. We quantified the average signal at both poles of the junctional ring within a region of interest. The newly added error bars indicate the standard deviation between pixel intensities within the ROI. The analysis has been done on immunofluorescent images, therefore a dynamic analysis over time is not possible.

In Figure 6c, we have analyzed the Myl9b-mCherry intensities and find that it is redistributed during a JBL cycle. The spatial distribution is evident from the heat-map and we have not included a standard deviation. Myl9b-mCherry levels are very heterogenous and is not possible to quantify intensities across samples. We have, however, included four more examples of Myl9b-mCherry distribution in Supplementary Figure 4. The patterns observed in these samples are consistent with those in Figure 6.

> *(6) Figure 5. The 'f' in the figure legend should be 'e' since there is no panel 'f'.*

We have corrected this.

> *(7) Figure 7. As the boundaries for proximal and distal junctions are not always clear, especially when Cdh5 appears as clusters, how do you determine where the two junctions are in order to measure the interjunctional space? Please offer a clearer explanation in the Methods.*

We have added the following in the M&M. “Junctional merging tracking Speed of junctional merge was evaluated by monitoring isolated junctional rings during DLAV formation. Inhibitor treatment Y-27632 (75 μM) or DMSO (1%) were applied 30 min before mounting. The same concentrations of chemicals were applied to the low-melting-point agarose mounting medium and the E3 medium on top of it before imaging and imaging the junctions for 10-15 min on an Olympus SpinSR spinning disc microscope. Distances were measured using Fiji software. In each frame, the interjunctional distance was defined as the maximum distance between the proximal and distal junctions. A line was manually drawn between the proximal and distal junctions in Fiji, and its length was recorded. The same proximal and distal junction landmarks were used consistently across all time points.”

> *(8) One would think that upon the inhibition of junctional mergence (by ROCK inhibition), actin polymerization would persist to push the distal junction forward to elongate the JBL. However, there is instead a decrease in junctional elongation (Figure 7b). Can the authors speculate why? Additionally, junction elongation can probably be achieved by continuous "pushing" of the distal junction alone (through actin polymerization). Can the authors speculate why there is a need/what is the benefit of merging proximal and distal junctions for junction elongation?*

These are all very interesting questions, but they are quite complex and would require extensive and speculative answers, which is outside the scope of this study. Nevertheless, here are a few quick thoughts on these issues.

(1) When endothelial cells elongate, they have to overcome tensile forces at the junctions (generated by the subjunctional actomyosin belt). JBL are providing a tractive and deforming force, which overcomes the tensile force and thus promotes junctional elongation.

(2) The distal junction is then providing an anchor to which the actin cytoskeleton can attach. The space between proximal and distal junction becomes a compartment of local actomyosin contraction, which provides the force for the ratchet to move the proximal junction forward junctional mergence.

(3) Thus, it is not the protrusion (pushing) itself that elongates the cell but the elongation of the junction (driven by actomyosin contraction)!

(4) The maintenance of the proximal junction is most likely needed to ensure endothelial integrity during the JBL cycles.

(5) How the frequency and the size of JBLs is regulated is not known. One possible player that might be involved is an internal clock mechanism (e.g. a feedback loop via small GTPases (such as Rac) Arp2/3 regulation). Another possibility is that JBL size is limited by it sweeping up basally localized VE-cadherin (in cis-configuration). Increasing cell-cell adhesion (by VE-cad trans-interactions between the JBL and the underlying cell) eventually stop the protrusion. It is also possible that an cell-autonomously controlled mechanism of F-actin polymerization (actin pulses) are involved in the regulation of the JBC cycle length.

> *(9) The animation showing the molecular mechanism of JBL function during endothelial junction elongation (Video 25) is very helpful in understanding the dynamic coupling between junctional proteins, actomyosin cytoskeleton, and junction remodelling. However, I wonder why there are no Myosin II proteins binding to the actin bundles during the merging of proximal and distal junctions (between 0:25 and 0:28), since this is one of the main findings by the authors in this study.*

Since we show two JBL cycles, we want to spread the information over both of them.

References:

Cao, J. and Schnittler, H. (2019). Putting VE-cadherin into JAIL for junction remodeling. J. Cell Sci. 132.

Cao, J., Ehling, M., März, S., Seebach, J., Tarbashevich, K., Sixta, T., Pitulescu, M. E., Werner, A. C., Flach, B., Montanez, E., et al. (2017). Polarized actin and VE-cadherin dynamics regulate junctional remodelling and cell migration during sprouting angiogenesis. Nat. Commun. 8, 1–20.

Chou, S. Z., Chatterjee, M. and Pollard, T. D. (2022). Mechanism of actin filament branch formation by Arp2/3 complex revealed by a high-resolution cryo-EM structure of the branch junction. Proc. Natl. Acad. Sci. U. S. A. 119, e2206722119.

Fernandez-Gonzalez, R., Simoes, S. de M., Röper, J. C., Eaton, S. and Zallen, J. A. (2009). Myosin II Dynamics Are Regulated by Tension in Intercalating Cells. Dev. Cell 17, 736–743.

Hetrick, B., Han, M. S., Helgeson, L. A. and Nolen, B. J. (2013). Small molecules CK-666 and CK-869 inhibit actin-related protein 2/3 complex by blocking an activating conformational change. Chem. Biol. 20, 701–712.

Kipcke, J. P., Odenthal-Schnittler, M., Aldirawi, M., Franz, J., Bojovic, V., Seebach, J. and Schnittler, H. (2025). TNF-α induces VE-cadherin-dependent gap/JAIL cycling through an intermediate state essential for neutrophil transmigration. Front. Immunol. 16,.

Law, A. L., Jalal, S., Pallett, T., Mosis, F., Guni, A., Brayford, S., Yolland, L., Marcotti, S., Levitt, J. A., Poland, S. P., et al. (2021). Nance-Horan Syndrome-like 1 protein negatively regulates Scar/WAVE-Arp2/3 activity and inhibits lamellipodia stability and cell migration. Nature Communications 2021 12:1 12, 5687-.

Malchow, J., Eberlein, J., Li, W., Hogan, B. M., Okuda, K. S. and Helker, C. S. M. (2024). Neural progenitor-derived Apelin controls tip cell behavior and vascular patterning. Sci. Adv. 10, 1174.

Munjal, A., Philippe, J. M., Munro, E. and Lecuit, T. (2015). A self-organized biomechanical network drives shape changes during tissue morphogenesis. Nature 524, 351–355.

Paatero, I., Sauteur, L., Lee, M., Lagendijk, A. K., Heutschi, D., Wiesner, C., Guzmán, C., Bieli, D., Hogan, B. M., Affolter, M., et al. (2018). Junction-based lamellipodia drive endothelial cell rearrangements in vivo via a VE-cadherin-F-actin based oscillatory cell-cell interaction. Nat. Commun. 9,.

Padrick, S. B., Doolittle, L. K., Brautigam, C. A., King, D. S. and Rosen, M. K. (2011). Arp2/3 complex is bound and activated by two WASP proteins. Proc. Natl. Acad. Sci. U. S. A. 108, E472–E479.

Sauteur, L., Krudewig, A., Herwig, L., Ehrenfeuchter, N., Lenard, A., Affolter, M. and Belting, H. G. (2014). Cdh5/VE-cadherin promotes endothelial cell interface elongation via cortical actin polymerization during angiogenic sprouting. Cell Rep. 9, 504–513.

Seebach, J., Klusmeier, N. and Schnittler, H. (2021). Autoregulatory “Multitasking” at Endothelial Cell Junctions by Junction-Associated Intermittent Lamellipodia Controls Barrier Properties. Front. Physiol. 11,.

Taha, A. A., Taha, M., Seebach, J. and Schnittler, H. J. (2014). ARP2/3-mediated junction-associated lamellipodia control VE-cadherin-based cell junction dynamics and maintain monolayer integrity. Mol. Biol. Cell 25, 245–256.

https://doi.org/10.7554/eLife.109264.2.sa0